ANALYSIS OF VOID FRACTION PHASE DISTRIBUTION OF GAS-LIQUID FLOW IN A HORIZONTAL PIPE USING WIRE MESH SENSOR DATA

A Thesis Presented to the Department of

Petroleum Engineering

The African University of Science and Technology

In Partial Fulfilment of the Requirements

For the Degree of

MASTER OF SCIENCE

By

Inkum Henry

Abuja, Nigeria

December, 2014

ANALYSIS OF VOID FRACTION PHASE DISTRIBUTION OF GAS-LIQUID FLOW IN A HORIZONTAL PIPE USING WIRE MESH SENSOR DATA

By

Inkum Henry

RECOMMENDED: ....

Supervisor, Dr. Mukhtar Abdulkadir

....

Professor Wumi Iledare

....

Dr. Alpheus Igbokoyi

APPROVED: ....

Head, Department of Petroleum Engineering

....

Chief Academic Officer

....

DATE

ABSTRACT

The scope of this work was to make detailed analysis of phase distribution in a horizontal pipe. This detailed analysis has been successfully carried out. Data obtained from wire mesh sensor (WMS) were used for the analyses. The operating fluid considered was an air/silicone oil mixture within a 6 m horizontal pipe with internal diameter of 0.067 m. The gas superficial velocities considered spans from 0.047 to 4.727 m/s, whilst liquid superficial velocities ranged from 0.047 to 0.4727 m/s. The wire mesh sensor (WMS) data obtained consist of the average cross-sectional and time average radial void fraction sensor with an acquisition frequency of 1000 Hz over an interval of 60 s. For the range of flow conditions studied, the average void fraction was observed to vary between 0.38 and 0.85. An analysis of the results shows that the major flow patterns observed in this study were found to be in slug and smooth stratified flow regime with the slug flow been the dominant one. At constant liquid superficial velocity, the void fraction increases with an increase in the gas superficial velocity. This observed trend in the horizontal void fraction is consistent with the observations made by (Abdulkadir et al., 2014) and (Abdulkadir et al., 2010) which were all in the vertical orientation. The performance of the void fraction correlations and their accuracies were judged in terms of percentage error and RMS error. Nicklin et al. (1962), Hassan (1995) and Kokal and Stanislav (1989) were judged as the best performing correlations and Greskovich and Cooper (1975) as the least. A cubic profile which was dependent on the gas superficial velocity was observed as the radial void fraction increases with gas superficial velocity. It was also obseved that for a given liquid superficial velocity, the frictional pressure drop increases with increase in both gas and mixture superficial velocities. Another finding made was that, even though Wu et al. (2001)'s model was proposed for vertical orientation with air and water used as the operating fluid, it could as well replicate the observed radial void fraction in the horizontal orientation. The experimental frequency was seen to increase with liquid superficial velocity but followed a sinusoidal trend with increase in gas superficial velocity.

DEDICATION

This thesis work is dedicated to my lovely wife, my beloved and partner Mrs. Gifty Inkum. You are a woman everyman would like to have. Thank you for loving me just as I am. Thank you for your love and kindness. I love you always.

ACKNOWLEDGEMENT

I would first and foremost like to give thanks to the almighty God for how far He has brought me in this life. I never thought I could be where I am now but He made it possible. I thank Him also for His protection from wicked and unreasonable men and also for being my shepherd throughout this many year of my life. Baba God, thank you.

I would like to also express my gratitude to my advisor Dr. Abdulkadir Mukhtar for his untiring support and guidance not only in this work and preparation of the manuscript but also throughout my entire graduate study. No words would be good enough to express my gratitude to my parents and all my family who have done everything to make my graduate studies possible. I will forever cherish their endless love and support.

A virtuous woman who can find? I am so glad that I found you and my mind would never change about you. Thank you for all the sacrifices you have made for me. I will be forever grateful to you my dear and lovely wife GINK. I love you so much.

TABLE OF CONTENTS

LIST OF FIGURES

LIST OF TABLES

CHAPTER 1
INTRODUCTION

1.1 Problem Definition

In this world system you would realize that as human as we are, we are not complex to understand as single units. For example, let us take the male species, you would realize that he is kind of burden free when he is single but as soon as he marries then he brings a burden of the wife and the children if he has one on himself, in the sense that he now has a lot of responsibilities relative to the time he was single. These increases in responsibilities are not peculiar to the man alone but also to the woman as well. There are therefore a lot of problems that arise as a result of the union between the man and the woman. If today they are not figurehting and threatening to divorce each other, tomorrow they may be quarrelling and insulting each other as to why they made such a wrong choice. Today, marriage has become like a besieged city, all those in it want to come out and all those who are out want to go in. It is amazing, isn't it?

These complex phenomenon that exist between a man and a woman co-existing in a marriage is the same complex phenomenon that can be observed from oil and gas which is transported together in a single pipe. Initially when an oil well is been produced, at a pressure at or above the bubble point pressure only oil is been produced which can be likened to a bachelor who is burden free but immediately the well is produced below bubble point pressure, gas begin to come out of solution, hence multiphase phenomenon and therefore the need to transport both oil and gas through the pipes.

The onshore and offshore production and transportation of oil and gas resources has always been a challenge within the energy industry, with engineers having to deal with the various technical and environmental challenges associated with multiphase flows. For example, in an offshore environment, it is economically preferable to

transport gas and liquid mixtures through a single flow line and separate them onshore (Abdulkadir et al., 2010). However, two-phase flow is an extremely complicated physical phenomenon occurring particularly in the petroleum industry during the production and the transportation of oil and gas due to its unsteady nature and high attendant pressure drop. This may eventually damage the pipe system, therefore the complexity of the potential flow regimes present within these pipelines has attracted considerable research interest to improve our understanding of two-phase flow phase distribution in a pipe system under various processing conditions. The spatial distribution of the phases inside the pipe and the pipe geometry play an extremely important role in the accurate determination of pressure gradient and flow hydrodynamic characteristics. The flow patterns and the void fraction are one of the key parameters in two phase flow. The two phase flow in vertical pipes is symmetrical about the pipe axis and is governed by the interaction between the liquid inertia, buoyancy, gravity and surface tension forces. However flow patterns and the void fraction in horizontal pipes is governed by the density segregation (Bhagwat and Ghajar, 2012).
A vital characteristic of two-phase flow is the presence of moving interfaces and the turbulent nature of the flow that make theoretical predictions of flow parameters greatly more difficult than in single-phase flow. Thus, experimental measurements play an important role in providing information for design, and supporting analysis of system behavior. Because of this, there is a real need to make certain measurements of void fraction distribution for model development and testing. As it happens, these quantities must also be measured for control and monitoring of industrial two phase systems.

Void fraction is an important variable in any two-phase flow system for determining pressure loss, liquid holdup and prediction of heat transfer (Abdulkadir et al., 2014). Significant amount of research has been done in the field of flow patterns and void fraction phase distribution in vertical pipes (both upward and downward orientation) and in an inclined system two phase flow, but amazingly no studies have been published for void fraction phase distribution in horizontal pipes in all the various pipe geometry and fluid properties of the various analysis.

In relation to investigations in vertical pipes (both upward and downward) two phase flow, (Golan, 1969), (Beggs, 1972), (Mukherjee, 1979), (Nguyen, 1975) and (Oshinowo and Charles, 1974) made studies in this area. (Oshinowo and Charles, 1974) presented a description of the differences observed in the vertical upward and downward two phase flow. In more recent times (Abdulkadir et al., 2014), (Abdulkadir et al., 2010), (Azzopardi et al., 2008), (Szalinski et al., 2010) and (ohnuki, 2000) also made studies concerning void fraction distribution in vertical pipes. The list goes on and on of countless number of researchers who have made studies and publications in phase distribution in vertical pipes irrespective of the various types of pipe geometry, fluid properties and flowing condition. This study therefore presents detailed evaluation of phase distribution in horizontal pipes using wire mesh sensor data.

1.2 Background Information

Throughout literature it can be observed that many publications have been made in vertical pipes. Considering this same studies in vertical pipes it can also be noticed that different types of pipe geometry (large and small pipe diameter, long and short pipe length), fluid properties (air/water and air/silicon oil, low viscous and highly viscous) and flow conditions were analyzed. From the many publications made on the detailed analyses of phase distribution in pipes, it can be concluded that they are skewed in the direction of vertical pipes. These findings have motivated me to do my analyses of the phase distribution in horizontal pipes since no much work has been done in that field. The following are some publications made on phase distribution in vertical pipes by various researchers with different kinds of pipe geometries, fluid properties and flow conditions from early times to recent times in order to confirm my assertions.

(Hasan, 1995) conducted an experiment and came out with a model for estimating void fraction in a downward direction of a vertical and inclined systems for two dominant flow regimes, bubbly and slug flow. He made use of the drift flux approach to determine the slip between the phases and the transition between the flow regimes. He concluded that for both bubbly and slug flow the effect of buoyancy, expressed by the terminal bubble-rise velocity, has the same magnitude as that for the case of upflow. He also found that the flow distribution parameter in bubbly flow appears to have the same value of 1.2 as in upflow. For slug flow, however, the flow parameter is represented by a somewhat lower value (1.12) than for upflow.

(Morooka et al., 1989) carried out an experimental study on void fraction in a simulated BWR fuel assembly. In their study, they made use of an advanced X-ray CT scanner in measuring void fraction of a vertical (4 × 4) rod bundle which was conducted in a steam-water two phase flow. They found out that the cross-sectional averaged void fraction data for the rod bundle that was obtained could be correlated by the Drift-Flux model and that the Zuber-Findlay correlation underestimates the data in a void fraction area of 80% or more. They attributed their findings to the fact that their data range over which their correlation was developed, does not cover the experimental range. Therefore, a modified correlation was developed based on their data.

(Akimoto and Ohnuki, 1996) also carried out an experimental study on developing air-water two-phase flow along a large vertical pipe and looking at the effect of air injection method on the development. The vertical pipe investigated was 0.48 m in diameter and 4.2 m of the ratio of length of the flow path. An extremely different flow structure in the developing region were realized when two air injection methods (porous sinter injection and nozzle injection) were adopted. They observed that no air slugs occupying the flow path were recognized in the experiment regardless of the air injection methods they used. At the end of their study they concluded that in the upper half of the test section, the effects of the air injection methods were small in respect of the shapes of the differential pressure distribution and the phase distribution, however in the lower half of the test section, the axial distribution of sectional differential pressure and the radial distribution of local void fraction showed peculiar distributions in relation to the air injection method adopted. They also compared their results to (Kotaoka, 1987)'s correlation and (Hills, 1976) correlations which showed that the bubble size distribution is considered to be affected by the ratio of length of the flow path, L/Dh.

(Prasser et al., 2001) carried out a study on the evolution of the two-phase flow in a vertical tube—decomposition of gas fraction profiles according to bubble size classes using wire-mesh sensors. A sequence of instantaneous gas fraction distributions in a cross section with a time resolution of 1200 frames per second and a spatial resolution of about 2–3 mm were used. The flow velocities were (up to 1–2 m/s). They concluded that the different behaviour of small and large bubbles in respect to the action of the lift force were in a mixture of small and large bubbles

(Manera et al, 2008) carried out a detailed comparison between wire-mesh sensors and conductive needle-probes for measurements of two-phase flow parameter. The measurements of two-phase flow parameters such as void-fraction, bubble velocities, and interfacial area density were performed in an upwards air–water flow at atmospheric pressure by means of a four-tip needle-probe and a wire-mesh sensor and both techniques were based on the measurement of the fluid conductivity. They found out that for a void-fraction and velocity measurements, similarity existed between the two methodologies for signal analysis. They concluded that the comparison between the two techniques showed a good agreement.

(Szalinski et al., 2010) carried out a comparative study of gas-oil and gas-water two-phase flow in a vertical pipe. A wire-mesh sensor was employed to study air/water and air/silicone oil two-phase flow in a vertical pipe of 67mm diameter and 6m length. The sensor was operated with a conductivity- measuring electronics for air/water flow and a permittivity-measuring one for air/silicone oil flow. Their experimental setup enabled a direct comparison of both two-phase flow types for the given pipe geometry and volumetric flow rates of the flow constituents. They used the time series of cross-sectionally averaged void fraction to determine characteristics in amplitude and frequency space. In a more three-dimensional examination, radial gas volume fraction profiles and bubble size distributions were processed from the wiremesh sensor data and compared for both flow types. Information from time series and bubble size distribution data was used to identify flow patterns for each of the flow rates studied.

(Bhagwat and Ghajar, 2011) carried out an experiment and in their study they presented an experimental results of the flow patterns and the void fraction measurements for vertical upward and downward two phase flow. They concluded that a definite difference in appearance existed in the interaction of the liquid inertia and the buoyancy force of the upward and downward two phase flow. Their analysis was based on 1208 and 909 experimental data points for upward and downward flows which showed a definite tendency of the variation of the void fraction with varying phase flow rates.

Last but not least, just recently (Abdulkadir et al., 2014) carried out an experimental study concerned with the phase distributions of gas–liquid multiphase flows experienced in a vertical riser. Scale experiments were carried out using a mixture of air and silicone oil in a 6 m long riser pipe with an internal diameter pipe of 67 mm. An analysis of the data collected concluded that the observed void fraction was strongly affected by the gas superficial velocity, whereby the higher the gas superficial velocity, the higher was the observed average void fraction. A comparison of the experimental data was performed against a published model to investigate the flow structure of air– water mixtures in a bubble column. A satisfactory report was observed for radial void fraction profile (mean relative error is within 5.7%) at the higher gas superficial velocities.

Amazingly none of these publications outlined above and other ones not mentioned were made in horizontal pipes, thus the endeavor of this study is to make a detailed analyses of the phase distribution in horizontal pipes using Wire Mesh Sensor Data (WMSD).

1.3 Aim and Objectives

The main aim and objectives of this work are:

1.3.1 Aim

The aim of this work is to provide a detailed analysis of phase distribution of gas-liquid flow experienced in a horizontal pipe.

1.3.2 Objectives

In order to achieve the aim of this study, the following objectives will be met:

1. The effect of gas and liquid superficial velocities on time averaged radial gas volume fraction profiles would be analyzed.
2. The experimental data will be compared to already existing empirical correlations in order to investigate how much they agree and to determine the best performing one.
3. Analysis would be made on the probability density function (pdf) of void fraction and radial time averaged void fractions at different air superficial velocities.
4. The pressure drop experienced in horizontal flow will be analyzed.
5. (Wu et al., 2001)'s published equation would be compared to the experimental time averaged radial void fraction.
6. Experimental frequency will be compared to empirical models and also to determine the effect the gas superficial velocity has on the experimental frequency.

1.4 Organization of the Study

To achieve those objectives, this report has been separated into five chapters. Following a brief introduction of the problem, the state of art of multiphase flow will be reviewed in Chapter II. This chapter will mention the available methods, conclude the recent development in this area and state the difficulty in further studies. The overview of the experimental facility will be stated in Chapter III, followed by the results obtained from experimental data and the corresponding analyses and discussions made in Chapter IV. Finally, thesis conclusions and recommendations for future work are stated in Chapter V.

CHAPTER 2
LITERATURE REVIEW

Two-phase gas-liquid flow is widely encountered in petroleum, chemical, civil and nuclear industries. In petroleum industry, those common problems include the calculation of the flow rate, pressure loss, and liquid holdup in the pipeline for multiphase flow in tubing design, gathering and separation system design, sizing of gas lines, heat exchanger design, and condensate line design (Brown, 1977).

The most unique characteristic of multiphase flow is phase distribution, which is very difficult to be characterized and predicted due to the existence of moving multi-boundary and turbulence. From very early times, researchers started to take advantage of flow regime for the qualitative description of phase distribution and the improvement of the accuracy of prediction. Almost all current models are based on the concept of flow regimes. For a specific system, the flow regime needs to be predicted by flow maps or flow regime transition theory. Then different flow models are used for the prediction of pressure drop and other parameters. The disadvantage of these models is that they create discontinuities and may induce divergence problem across the transition regions as the results of switching from one flow model to another one. To avoid this problem, the interpolation technique or some special criteria was used (Gomez et al., 1999; Petalas & Aziz, 2000).

In vertical pipes, two-phase flow can be classified into four flow regimes: bubble flow, slug flow, churn flow and annular flow (Figure 1.1). The models for bubble flow and annular flow are more developed than slug and churn flows in that the latter patterns have highly irregular interface with stronger unsteady nature (Xiaodong, 2005). However, slug flow appears in very wide range of flowing conditions and very common in wellbores. The pseudo-periodical character of slug flow has attracted so many researchers to study it using various methods including correlations, one-dimension mechanistic methods (Fernandes et al., 1983; Sylvester, 1987; and Orell and Rembrand, 1986; Taitel and Barnea, 1990) to multi-dimension exact solution of continuum equations and momentum equations (Mao and Dukler, 1989; Clarke and Issa, 1997; Kawaji et al., 1997; Anglart and Podowski, 2000).

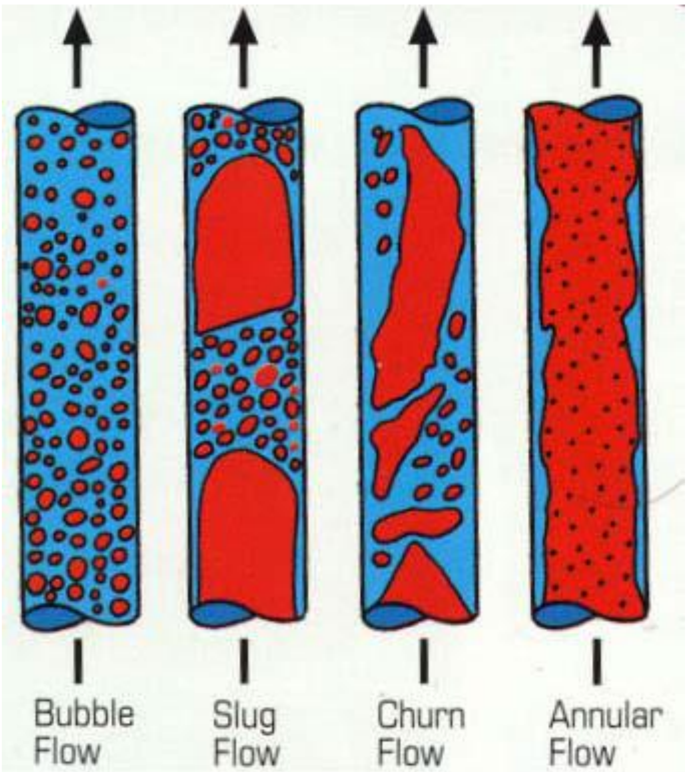

Figure 2.1: Different Flow Regimes in Vertical Pipes

Since the beginning of multiphase research in 1940's, hundreds of papers have been published in this area. The technology of multiphase flow has undergone significant changes, especially in recent years with the advancement of experimental facilities and numerical calculation ability. Several researchers reviewed the state of art of multiphase flow from different prospective. Brill (1987, 1992) reviewed the historical development of multiphase flow in petroleum engineering. Worner (2003) gave an insight in the physics of multiphase flow, its mathematical description, and its physical modeling for numerical computation by computer codes. Taitel (1995) concluded the advances of mechanistic modeling in two phase flow. Taitel & Barnea (1990) and Fabre & Line (1992) reviewed the mechanistic modeling of slug flow and various options of modeling the hydrodynamic parameters and pressure drop by using a unified approach applicable for the vertical, horizontal, as well as the inclined pipes. In order to improve the method of predicting multiphase, literatures were reviewed according to modeling methodology. Papers reviewed cover several areas, including petroleum, chemical, nuclear and mechanical engineering.

Basically, the methodology applied in multiphase flow can be classified as three categories: Empirical correlations, Mechanistic models and Numerical models. Empirical correlations develop simplified relations among important parameters which must be evaluated by experimental data. The empirical correlations do not address too much detail behind and behaves like a black box although sometimes slippage and flow regimes are considered. They can yield excellent results but only limited to the same conditions as the experiments. According to Taitel (1995), mechanistic models approximate the physical phenomenon by taking into consideration the most important processes and neglecting other less important effects that can complicate the problem but not add accuracy considerably. Furthermore, numerical models introduce multi-dimensional Navier-Stokes equations for multiphase flow. More detailed information can be obtained from numerical models such as multi-dimensional distribution of phases, dynamic flow regime transition and turbulent effects. The division among these approaches is not always clearly defined and the definition may depend on the specific terminology in specific area. Some empirical correlations consider slippage effect and flow regime, which are the most important phenomenon in multiphase flow. On the other hand, both the mechanistic models and numerical models have to utilize some inputs based on correlations due to the limitations of the current knowledge.

2.1 Complexity of Multiphase Flow

Phase is a thermodynamic definition for the state of matter, which can be solid, liquid or gas. Multiphase flow happens when the concurrent movement of liquids, gases or/and solids simultaneously in the pipes. The flow behavior of multiphase flow is pretty complex due to the co-existence of turbulence effect and moving boundary between different phases.

The interface between different phases may exit in various configureurations, known as flow patterns, which is the most unique characteristic of multiphase flow. The specific flow pattern depends on the flowing conditions, fluid properties and pipe geometries. The simplest classification is to use three regimes: separated flow, intermittent flow and distributed flow. Each of them can be further classified as several flow patterns. For example, segregated flow includes smooth stratified, wavy stratified and annular flow. Flow patterns in various pipes are shown in Figure 2.2. However, flow patterns are a subjective and qualitative concept. There is no way to incorporate it into mathematical equations as a parameter. The predicted results usually show some discontinuity between different patterns which is naturally smooth and continuous.

Another important phenomenon making the complexity of multiphase flow is that the gas tends to flow faster than liquid phase which is called slippage. The slippage effect makes the mixing fluid properties dependent on flowing conditions, fluid properties and pipe geometry. Therefore there is no way to obtain the fluid properties for the mixture of liquid and gas using simple methods.

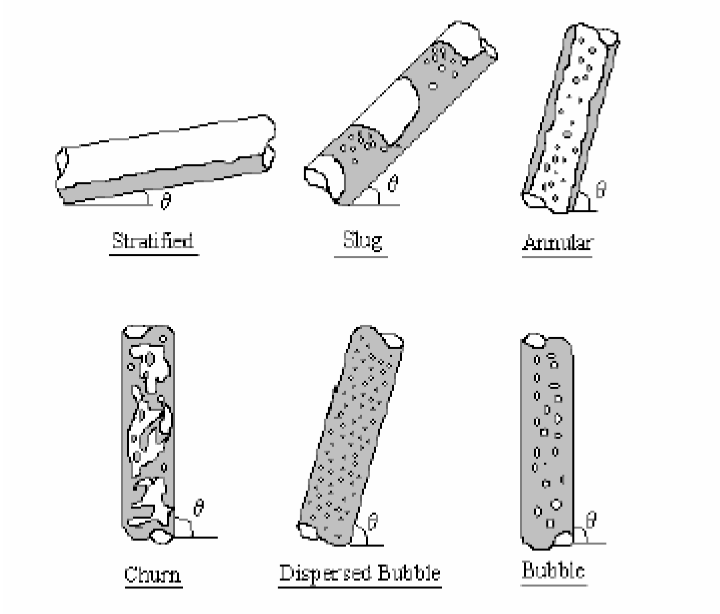

Figure 2.2: Flow Patterns in Pipes

All independent parameters affecting the flow behavior include the velocity, the viscosity, the surface tension, the density for liquid and gas respectively, and the diameter, the length, the inclined angle and roughness of the pipe. Dimension analysis is a powerful tool to construct new empirical correlations. Brill (1987) argued that the first and perhaps only exhaustive dimensional analysis of multiphase flow in pipes was performed by Duns and Ros (1963). They constructed 10 independent dimensionless groups and concluded that four of them were important for the prediction of horizontal multiphase flow according to experimental data.

Worner (2003) analyzed the forces in multiphase flow and their magnitude. The important forces acting in multiphase flow include pressure force, inertia force, gravity force, buoyancy force and surface tension force. From these six fundamental forces, five independent non-dimensional groups can be derived, which are Reynolds number, Euler number, Froude number, Weber number, Eotvos number. Further, some more groups can be defined, including Capillary number, Morton number, and the density and viscosity ratio of the phases. To construct a general correlation involving all these groups will require large amount of experimental data which are too difficult to collect.

2.2 Flow Patterns in Horizontal Pipes

When two or more phases flow simultaneously in pipes, the flow behaviour is much more complex than for single flow. The phases tend to separate because of differences in density. Shear stresses at the pipe wall are different for each phase as a result of their different densities and viscosities. Expansion of the highly compressible gas phase with decreasing pressure increases the in-situ volumetric flow rate of the gas. As a result, the gas and liquid phases normally do not travel at the same velocity in the pipe. The flow patterns that exist during two or more phase fluid movement depend on the relative magnitude of the forces that act on the fluids. Buoyancy, turbulence, inertia and surface tension forces vary significantly with flow rates, pipe diameter, inclination angle and fluid properties of the phases.

Two phase flow patterns in horizontal tubes are similar to those in vertical flows but the distribution of the liquid is influenced by gravity that acts to ensure the liquid is confined at the bottom of the tube and the gas at the top. Flow patterns for co-current flow of gas and liquid in a horizontal pipe are characterized as follows:

(i) Bubbly Flow. The gas bubbles are dispersed in the liquid with a high concentration of bubbles in the upper half of the pipe due to their buoyancy. When shear forces are dominant, the bubbles tend to disperse uniformly in the pipe. In horizontal flows, the regime typically only occurs at high mass flow rates.

(ii) Stratified Flow. At low liquid and gas velocities, complete separation of the two phases occurs. The gas goes to the top and the liquid to the bottom of the tube, separated by an undisturbed horizontal interface. Hence, the liquid and gas are fully stratified in this regime.

(iii) Stratified-Wavy Flow. Further increasing the gas velocity, these interfacial waves become large enough to wash the top of the tube. This regime is characterized by large amplitude waves intermittently washing the top of the tube with smaller amplitude waves in between. Large amplitude waves often contain entrained bubbles. The top wall is nearly continuously wetted by the large amplitude waves and the thin liquid films left behind. Intermittent flow is also a composite of the plug and slug flow regimes. Those sub-categories are characterized as follows:

(iv) Plug Flow. This flow regime has liquid plugs that are separated by elongated gas bubbles. The diameters of the elongated gas bubbles are smaller than the tube, such that, the liquid phase is continuous along the bottom of the tube below the elongated bubbles. Plug flow is also sometimes referred to as elongated bubble flow.

(v) Slug Flow. At higher gas velocities, the diameters of elongated bubbles become similar in size to the channel height. The liquid slug separating such elongated bubbles can also be described as large amplitude waves.

(vi) Annular Flow. At even larger gas rates, the liquid forms a continuous annular film around the perimeter of the tube, similar to that in vertical flow but the liquid film is thicker at the bottom than the top. The interface between the liquid annulus and the vapour core is distributed by small amplitude waves and droplets may be dispersed in the gas core. At high gas fractions, the top of the tube with its thinner film becomes dry first, so that the annular film covers only part of the tube perimeter and thus this is then classified as stratified-wavy flow.

- **Mist Flow.** Similar to vertical flow, at very high gas velocities, all the liquid may be stripped from the wall and entrained as small droplets in the continuous gas phase (Engineering Data Book III, 2007).

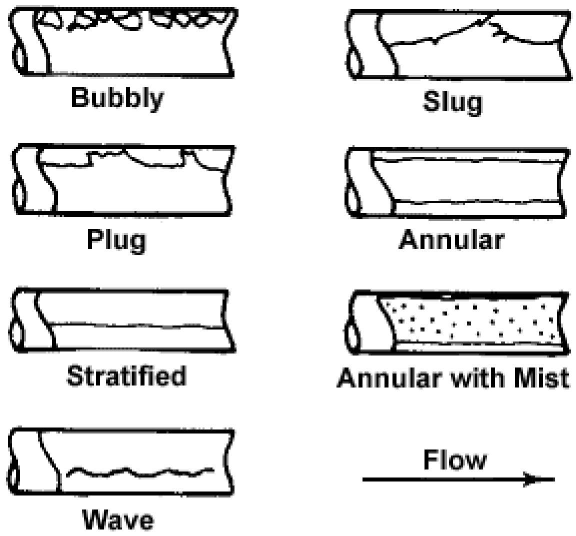

Figure 2.3. Two-phase flow patterns in horizontal flow.

2.3 Flow Patterns in Vertical Tubes

For co-current upflow of gas and liquid in a vertical tube, the liquid and gas phases distribute themselves into several recognizable flow structures. These are referred to as flow patterns and they are depicted in Figure 2.4 and can be described as follows:

(i) Bubbly flow: Numerous bubbles are observable as the gas is dispersed in the form of discrete bubbles in the continuous liquid phase. The bubbles may vary widely in size and shape but they are typically nearly spherical and are much smaller than the diameter of the tube itself.

(ii) Slug flow: With increasing gas void fraction, the proximity of the bubbles is very close such that bubbles collide and coalesce to form larger bubbles, which are similar in dimension to the tube diameter. These bubbles have a characteristic shape similar to a bullet with a hemispherical nose with a blunt tail end. They are commonly referred to as Taylor bubbles after the instability of that name. Taylor bubbles are separated from one another by slugs of liquid, which may include small bubbles. Taylor bubbles are surrounded by a thin liquid film between them and the tube wall, which may flow downward due to the force of gravity, even though the net flow of fluid is upward.

(iii) Churn flow: Increasing the velocity of the flow, the structure of the flow becomes unstable with the fluid traveling up and down in an oscillatory fashion but with a net upward flow. The instability is the result of the relative parity of the gravity and shear forces acting in opposing directions on the thin film of liquid of Taylor bubbles. This flow pattern is in fact an intermediate regime between the slug flow and annular flow regimes. In small diameter tubes, churn flow may not develop at all and the flow passes directly from slug flow to annular flow. Churn flow is typically a flow regime to be avoided in two-phase transfer lines, such as those from a reboiler back to a distillation column or in refrigerant piping networks, because the mass of the slugs may have a destructive consequence on the piping system.

(iv) Annular flow: Once the interfacial shear of the high velocity gas on the liquid film becomes dominant over gravity, the liquid is expelled from the center of the tube and flows as a thin film on the wall (forming an annular ring of liquid) while the gas flows as a continuous phase up the center of the tube. The interface is disturbed by high frequency waves and ripples. In addition, liquid may be entrained in the gas core as small droplets, so much so that the fraction of liquid entrained may become similar to that in the film. This flow regime is particularly stable and is the desired flow pattern for two-phase pipe flows.

(v) Wispy annular flow: When the flow rate is further increased, the entrained droplets may form transient coherent structures as clouds or wisps of liquid in the central vapour core.

(vi) Mist flow: At very high gas flow rates, the annular film is thinned by the shear of the gas core on the interface until it becomes unstable and is destroyed, such that all the liquid in entrained as droplets in the continuous gas phase, analogous to the inverse of the bubbly flow regime. Impinging liquid droplets intermittently wet the tube wall locally. The droplets in the mist are often too small to be seen without special lighting and/or magnification.

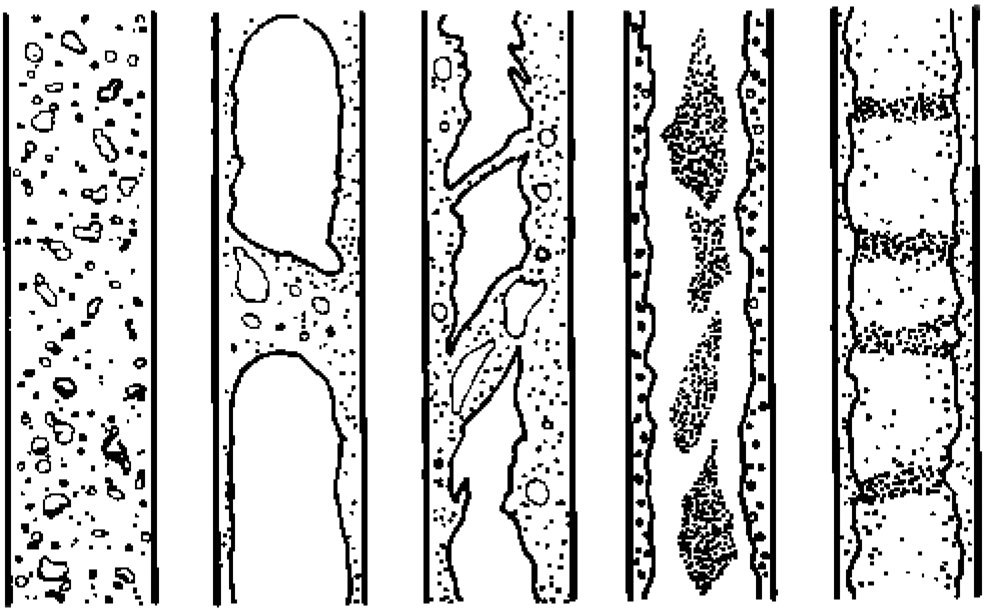

Figure 2.4: Two-phase flow patterns in vertical upflow.

2.4 Flow Pattern Maps

Flow patterns have an important influence on prediction of the void fraction, flow boiling and convective condensation heat transfer coefficients, and two-phase pressure drops. The prediction of flow pattern transitions and their integration into a flow pattern map for general use is thus of particular importance to the understanding of two-phase flow phenomena and design of two-phase equipment.

For vertical tubes, the flow pattern maps of Fair (1960) and Hewitt and Roberts (1969) are those most widely recommended for use. For horizontal tubes, the methods of Taitel and Dukler (1976) and Baker (1954) are widely used. The more recent flow pattern map of Kattan, Thome and Favrat (1998a) and its more subsequent improvements, which was developed specifically for small diameter tubes typical of shell-and-tube heat exchangers for both adiabatic and evapourating flows, is that recommended here for heat exchanger design. Another version of their map has also been proposed by El Hajal, Thome and Cavallini (2003) for intube condensation.

Shell side flow patterns and flow patterns maps have received very little attention compared to intube studies. Qualitative and quantitative attempts have been made to obtain flow pattern maps, but to date no method has been shown to be of general application.

The analysis of single-phase flow is made easier if one can establish that the flow is either laminar or turbulent and whether any separation or secondary flow effect occurs. This information is equally important in the study of gas-liquid flow. However, perhaps of greater importance in the latter case is the topology or geometry of the flow, i.e. the corresponding flow patterns or flow regimes.
Figure 2.5 shows a schematic representation of a horizontal tubular channel heated by a uniform low heat flux and fed with liquid just below the saturation temperature.

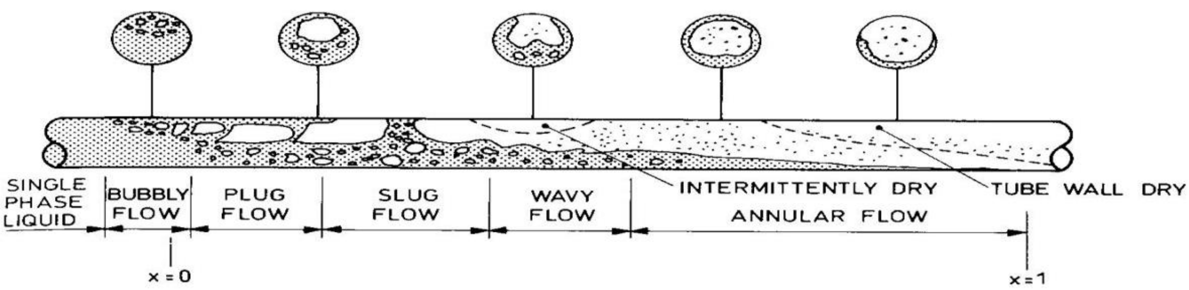

Figure 2.5: Flow patterns during evaporation in a horizontal tube (Collier and Thome, 1994)

To predict the local flow pattern in a tube, a flow pattern map is used. These are an attempt, on a two-dimensional graph, to separate the space into areas corresponding to the various flow regimes. It should be pointed out that the flow pattern is also influenced by a number of secondary variables but it is not possible to represent their influence using only a two-dimensional plot. One should be aware that transition curves on flow pattern maps should be considered as transition zones analogous to that between laminar and turbulent flows.

One of the greatest challenges of two-phase flow computations lies in the modeling of flow regime transitions, because a flow regime transition is difficult to predict and have a tremendous impact on the characteristics of the flow. At comparable flow rates, different flow regimes can be characterized by a quite different holdup, pressure drop, gas-liquid friction or sound velocity. For low gas densities for example, the transition from stratified to slug flow can result in a discontinuity in the liquid holdup.

The modeling of the transition between stratified and slug flow represents indeed a certain challenge, because of its chaotic nature, and because of the great variety of slug initiation mechanisms. Slugs can be initiated due to liquid accumulation at the low points of the pipe until the liquid forms a blockade which will travel down the pipe as a slug. If the upstream gas compressibility is high enough however, the slug formed at a low point of the pipe will not be expelled directly and the inlet pressure will increase as the gas accumulates upstream of the slug. When the upstream pressure is high enough to remove the slug, all the accumulated liquid and gas finally exits the pipe in a blow-out phase characterized by very high velocities. Then the liquid starts to accumulate again at the low point and a new cycle is started. Such phenomenon is called severe slugging and can be seen as the most extreme expression of slug flow. Another mechanism for the transition from stratified to slug flow is the sometimes quite slow growth of small perturbations at the gas-liquid interface due to the hydrodynamic instability of stratified flow at those conditions. The combined destabilizing effect of the friction forces and of the Bernoulli suction force will indeed lead to the formation and growth of interfacial waves until a slug is initiated. Slugs can also be initiated due to some operational transients, for example when the inlet gas flow rate is quickly increased. System - dependent effects can also play an important role: when a previously initiated slug leaves the pipe, the pressure within the pipe decreases and the gas in excess is evacuated. As a consequence, the gas velocities within the pipe increases, which can under certain circumstances, trigger a slug initiation. This phenomenon was observed in particular by Kristiansen (2004).

The effect of fluid properties or pipe geometry on the flow regimes is either unknown or is shown as a series of such flow pattern maps. For instance, the influence of pipe diameter and inclination on flow regime has to be deduced from flow maps. This is an essential point when applying flow pattern maps in complex pipe systems having relatively small length over diameter ratios. In these cases, the flow pattern may often differ from the pattern in long pipes with fully developed flows; as a result, the usual flow maps are of very limited use (Abdulkadir, 2011).

Additionally, the distinctions between different flow regimes are not always very clear and transitions difficult to observe accurately. Therefore, the transition lines have to be interpreted as a best estimate or most likely option of where the actual transition takes place, and the flow maps applied with care. The following are some flow pattern maps as espoused by different researchers.

2.4.1 Kristiansen Flow Pattern Map

A schematic flow map taken from Kristiansen (2004) indicates the prevailing flow regime for a given gas superficial velocity U_{sg} (defined as the ratio between the gas volume flow rate and the pipe cross-sectional area) and liquid superficial velocity U_{sl} . The influence of the pipe inclination (β) is the angle between the pipe and the horizontal, a negative value indicating a downward inclination) and of the pressure on the transition between stratified and slug flow is also shown in figure 2.5.

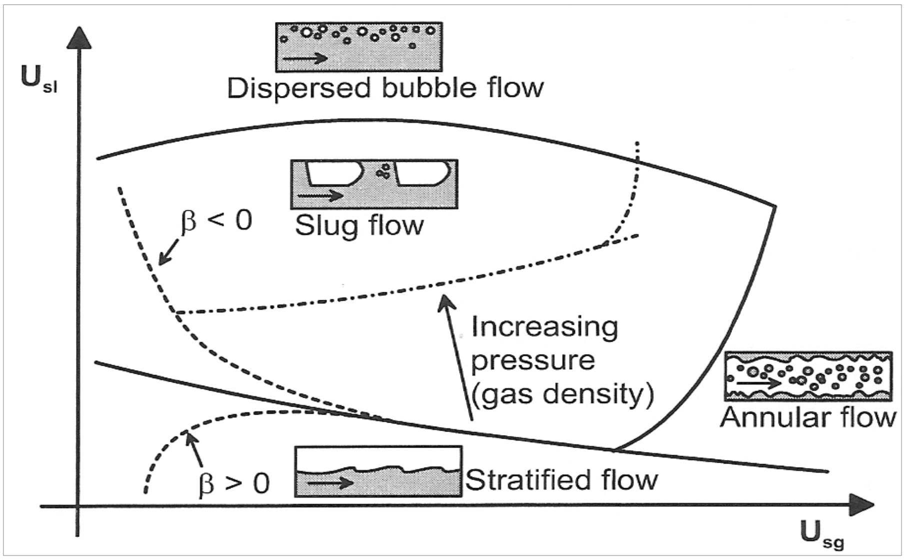

Figure 2.6: Simplified flow map (Kristiansen, 2004)

2.4.2 Baker Flow Pattern Map

The Baker (1954) map for horizontal two-phase flow in tubes shown in Figure 2.10 is presented in both SI and English units. To utilize the map, first the mass velocities of the liquid and vapour must be determined. Then his parameters λ and ψ are calculated. The gas-phase parameter λ is:

$$\lambda = \left(\frac{\rho_G}{\rho_{air}} \frac{\rho_L}{\rho_{water}} \right)^{1/2} \tag{2.1}$$

and the liquid-phase parameter ψ is:

$$\psi = \left(\frac{\sigma_{water}}{\sigma} \right) \left[\left(\frac{\mu_L}{\mu_{water}} \right) \left(\frac{\rho_{water}}{\rho_L} \right)^2 \right]^{1/3} \tag{2.2}$$

Where ρ_G, ρ_L, μ_L and σ are properties of the fluid and the reference properties are:

$$\rho_{water} = 1000 kg/m^3$$
$$\rho_{air} = 1.23 kg/m^3$$
$$\mu_{water} = 0.001 Ns/m^2$$
$$\sigma_{water} = 0.072 N/m$$

The values of the x-axis and y-axis are then determined to identify the particular flow regime.

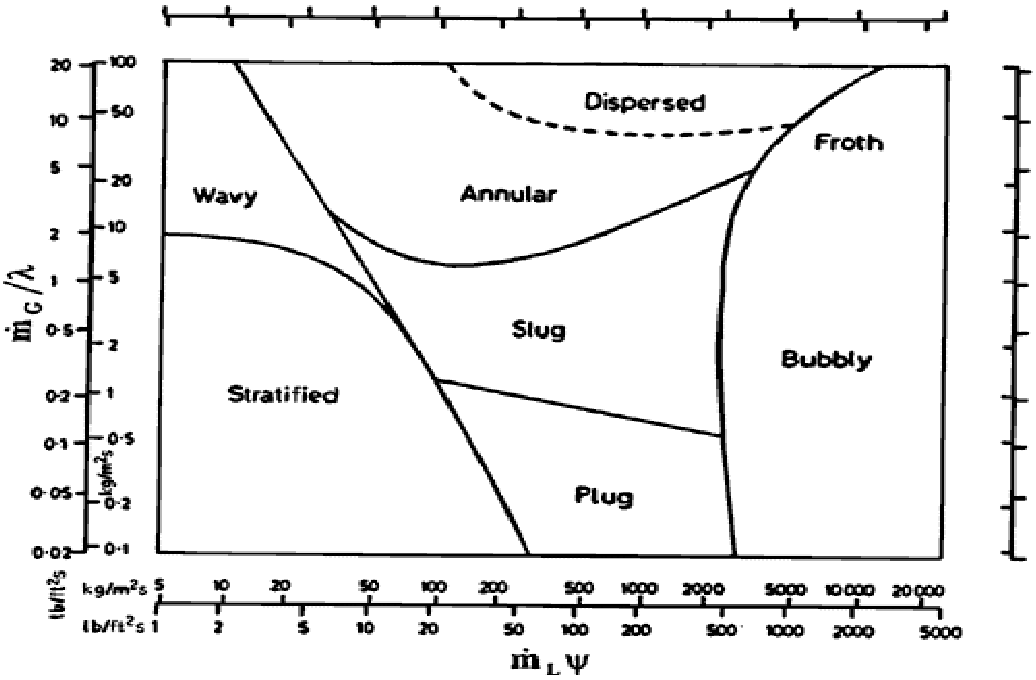

Figure 2.7: **Two-phase flow pattern map of Baker (1954) for horizontal tubes.**

2.4.3 Taitel and Dukler Flow Pattern Map

The Taitel and Dukler (1976) map for horizontal flow in tubes shown in Figure 2.11 is based on their analytical analysis of the flow transition mechanisms together with empirical selection of several parameters. The map uses the Martinelli parameter X, the gas Froude number Fr_G and the parameters T and K and is composed of three graphs. The Martinelli parameter is

The gas-phase Froude number is:

$$Fr_G = \frac{m_G}{[\rho_G(\rho_L - \rho_G)d_i g]^{1/2}} \qquad 2.3$$

Their parameter T is:

$$T = \left[\frac{(|dp/dz|)}{g(\rho_L - \rho_G)} \right]^{1/2} \qquad 2.4$$

Where g is the acceleration due to gravity $\left(g = 9.81 m/s^2\right)$. Their parameter K is:

$$K = Fr_G \, \mathrm{Re}_L^{1/2} \qquad 2.5$$

Where the liquid-phase and vapour-phase Reynolds numbers are:

$$\mathrm{Re}_L = \frac{\dot{m}_L d_i}{\mu_L} \qquad 2.6$$

$$\mathrm{Re}_G = \frac{\dot{m}_G d_i}{\mu_G} \qquad 2.7$$

The pressure gradient of the flow for phase k (where k is either L or G) is:

$$(dp/dz)_k = -\frac{2 f_k m_k^2}{\rho_k d_i} \qquad 2.8$$

For $\mathrm{Re}_k < 2000$, the laminar flow friction factor equation is used:

$$f_k = \frac{16}{\mathrm{Re}_k} \qquad 2.9$$

For $\mathrm{Re}_k > 2000$, the turbulent flow friction factor equation is used (even for the transition regime from 2000 to 10,000):

$$f_k = \frac{0.079}{\mathrm{Re}_k^{1/4}} \qquad 2.10$$

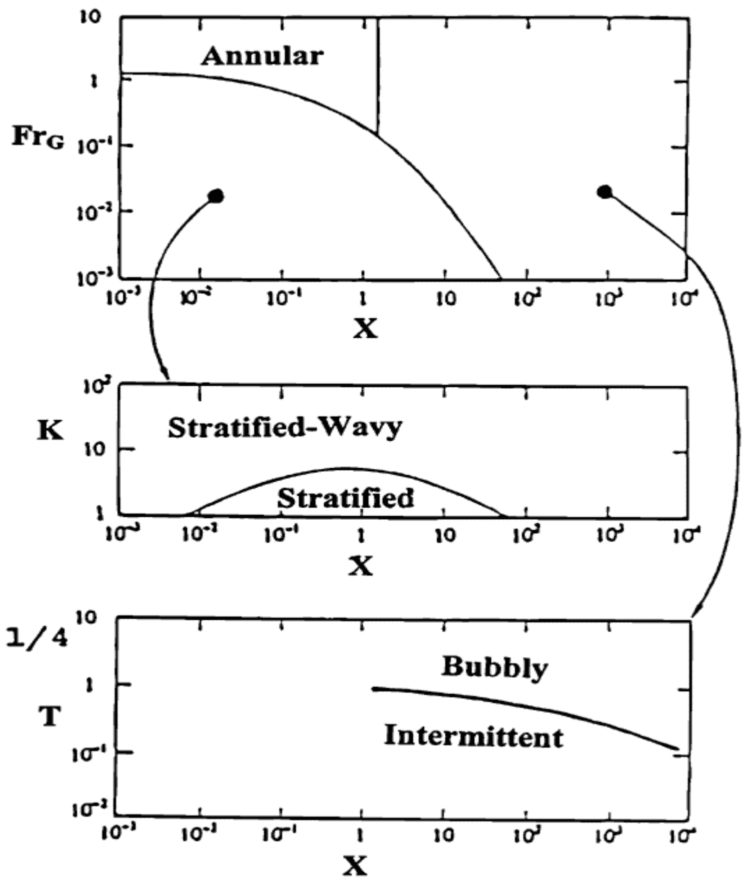

Figure 2.8: **Two-phase flow pattern map of Taitel and Dukler (1976) for horizontal tubes.**

To implement the map, one first determines the Martinelli parameter X and Fr_G. Using these two parameters on the top graph, if their coordinates fall in the annular flow regime, then the flow pattern is annular. If the coordinates of Fr_G and X fall in the lower left zone of the top graph, then K is calculated. Using K and X in the middle graph, the flow regime is identified as either stratified-wavy or as fully stratified. If the coordinates of Fr_G and X fall in the right zone on the top graph, then T is calculated. Using T and X in the bottom graph, the flow regime is identified as either bubbly flow or intermittent (plug or slug) flow.

These flow pattern maps were all developed for adiabatic two-phase flows but are often extrapolated for use with the diabatic processes of evapouration or condensation. As with any extrapolation, this may or may not produce reliable results.

For a description of flow pattern transition theory, a good review was presented by Taitel (1990).

2.5 Void Fraction Correlation

In facilitating better understanding of this manuscript, it is worthwhile to highlight some of the most common terminologies and definitions of parameters that would be encountered throughout this work.

Void fraction is defined as the volume of space the gas phase occupies in a given two phase flow in a pipe, hence for a total pipe cross sectional area of A; the void fraction is given by

$$\alpha = \frac{A_G}{A} \qquad 2.11$$

Liquid holdup is the complement of the void fraction in the pipe, i.e., it is the remaining volume of space occupied by the liquid phase. Thus, liquid holdup is

$$R_L = 1 - \alpha = \frac{A_L}{A} \qquad 2.12$$

The quality of the mixture, x , in the isothermal flow case we are considering here is taken as the input mass of the gaseous phase to that of the total mixture mass of m, hence

$$x = \frac{m_G}{m_M} \qquad 2.13$$

The slip ratio, S, is defined as the ratio of the actual velocities between the phases. A slip ratio of unity for a mixture being the homogeneous case where it is assumed that both phases travel at the same velocity. The slip ratio is defined as

$$S = \frac{U_G}{U_L} \qquad 2.14$$

The superficial gas, U_{SG},and liquid , U_{SL} , velocities are defined as the velocities of the gas or liquid phase in the pipe assuming the flow is a single phase in either gas or liquid respectively.

From the definitions given above and writing conservation of mass for each phase and total flow, we can define the relationships

$$U_G = \frac{U_{SG}}{\alpha} \qquad 2.15$$

$$U_L = \frac{U_{SL}}{1-\alpha} \qquad 2.16$$

$$\frac{x}{1-x} = \left(\frac{\rho_G}{\rho_L}\right)\left(\frac{U_{SG}}{U_{SL}}\right) \qquad 2.17$$

Having given the basic definitions of the most important and frequently used parameters in two phase flow in relation to void fraction, we now move on to presenting the correlations

Different void fraction (liquid holdup) correlations which appeared from the early 1960s to date collected from the open literature are presented here. The total number of correlations collected is more than 10. These correlations were developed from theoretical and mostly experimental investigations under various operating conditions. In presenting the correlations, different criteria were sought into which the developed correlations might conveniently fall.

As the complex nature of two phase flow has not yielded to any theoretical formulation of a particular flow pattern analysis let alone a general one, it can be observed from a literature search that the trend in correlation development is becoming more geared towards a specific area of particular interest which in effect has resulted in correlations for a specific flow regime. Hence, division along the type of flow pattern dependency is a logical step.

Finally, it is imperative to mention here that by nature all the empirical correlations have some sort of limitations, even though not explicitly reported by their authors. This is due to the very fact that they were fitted to given data sets which in turn depend on the inherent physical limitations of the experiment under which the data was collected. Therefore, rather than going after physical parameters(inclination angles, mass flow rates etc) which are too narrow or subjective criteria like flow pattern upon which there is no firm consensus to this date, we have decided to follow the work of Vijayan et al.(2000) to classify the correlations into four categories. These are:

1. Slip ratio correlations
2. $K\alpha_H$ correlations
3. Drift flux correlations
4. General void fraction correlations

A brief description of these categories and some correlation that falls into each of them are given below:

2.5.1 Slip ratio correlations

These correlations are of the form

$$\alpha = \frac{1}{1+S\left(\frac{1-x}{x}\right)^{b}\left(\frac{\rho_G}{\rho_L}\right)^{c}} \qquad 2.18$$

The most simple of all the correlations with a theoretical background and the assumption that the gas and liquid velocities are equal or there is no slip between them is the Homogeneous model or the no-slip correlation.

2.5.2 Kα_H Correlations

The other category of void fractions are those which are a constant multiple or some function (Isbin and Biddle, 1979) of the no slip (homogeneous) void fraction correlation.

In an effort to predict the void fraction taking into consideration the non-homogeneous nature of the two phase flow, Armand (1946) gave a correlation in the early days of two phase flow research and is one of the first few correlations to be developed and is given as

$$\alpha = 0.833\alpha_H \qquad 2.19$$

Bankoff (1960) correlation is developed from analysis on a single fluid with variable density and velocity profile for vertical flow. The original form of the equation is

$$\frac{1}{x} = 1 - \frac{\rho_L}{\rho_G}\left(1 - \frac{K_B}{\alpha}\right) \qquad 2.20$$

$$K_B = 0.71 + \left(1.45 \times 10^{-2}\right)P \quad \text{P in MPa} \qquad 2.21$$

Greskovich and Cooper (1975) developed a correlation from air water data for inclined flows. It was noted that the data showed little diameter dependency above 2.54cm but was considerably dependent on inclination angle

$$\frac{1}{\left[1 - 0.671\left(\left(\sin\theta\right)^{0.263} \Big/ Fr^{0.5}\right)\right]}\alpha_H \qquad 2.22$$

2.5.3 Drift flux correlations

This type of correlations are based on the work of Zuber and Findlay (1965) where the void fraction can be predicted taking into consideration the non-uniformity in flows and the difference in velocity between the two phases. This model is good for any flow regime. It has the general expression given by

$$\alpha = \frac{U_{SG}}{C_O U_M + U_{GM}} \qquad 2.23$$

where C_o is the distribution parameter and $U_{GM} = U_G - U_M$ is the slip velocity

Correlations that fall under this category are given below;

Nicklin et al. (1962) in an experiment done in 25.4mm (1 in) diameter vertical tube, produced an expression for the prediction of bubble velocity from which the void fraction could also be backed out. The constant 1.2 in the expression is said to be accurate for Reynolds numbers greater than 8000 and approximate for lesser values. The expression for the correlation is

$$\alpha = \frac{U_{SG}}{1.2U_M + 0.35\sqrt{gD}} \qquad 2.24$$

Hughmark (1965) The Hughmark correlation for the insitu liquid volume fraction was developed for vertical flow but it may also be applied to horizontal flow as confirmed by Dukler et al. The expression for the correlation is

$$\alpha = \frac{U_{SG}}{1.2(U_{SL} + U_{SG})} \qquad 2.25$$

Kokal and Stanislav (1989) correlated their air-oil experimental data in horizontal and near horizontal (±9°) pipe using the drift flux relation and recommended their correlation for all flow regimes. It is given as

$$\alpha = \frac{U_{SG}}{1.2U_M + 0.345\left[\frac{gD(\rho_L - \rho_G)}{\rho_L}\right]^{1/2}} \qquad 2.26$$

Clark and Flemmer (1985)

$$\varepsilon = \frac{U_{SG}}{1.17U_M + 1.53\left(g\sigma\left(\frac{\rho_L - \rho_G}{\rho_L{}^2}\right)\right)^{0.25}} \qquad 2.27$$

Cai et al. (1997)

$$\varepsilon = \frac{U_{SG}}{1.185U_M + 1.53\left(g\sigma\left(\frac{\rho_L - \rho_G}{\rho_L{}^2}\right)\right)^{0.25}} \qquad 2.28$$

Greskovich and Cooper (1975)

$$\varepsilon = \frac{U_{SG}}{1.0U_M + 0.671\sqrt{gD}(\sin\theta)^{0.263}} \qquad 2.29$$

Hassan (1995)

$$\varepsilon = \frac{U_{SG}}{1.12U_M + 0.345\sqrt{gD\left(1 - \frac{\rho_G}{\rho_L}\right)}} \qquad 2.30$$

Bankoff (1960)

$$\varepsilon = K_o \frac{X}{\left\{X + \frac{\rho_G}{\rho_L}(1 - X)\right\}} \qquad 2.31$$

$$K_o = 0.71 + 0.0001372P$$

P in MPa

Zuber-Findlay (1965)

$$\varepsilon = \frac{X}{C_o\left\{X + \frac{\rho_G}{\rho_L}(1-X)\right\} + \frac{\rho_G V_{gF}}{G}} \qquad 2.32$$

$$V_{gF} = 1.41\left[\frac{\sigma(\rho_L - \rho_G)}{\rho_L{}^2}\right]^{0.25} \qquad 2.33$$

$$C_o = 1.13$$

Ahmad (1964)

$$\varepsilon = \frac{1}{1+\left(\frac{1}{X}-1\right)\left(\frac{\rho_G}{\rho_L}\right)S} \qquad 2.34$$

$$S = \left(\frac{\rho_L}{\rho_G}\right)^{0.205}\left(\frac{GD}{\mu_L}\right)^{-0.0106}$$

2.6 Void Fractions in Two-Phase Flows

The void fraction ε is one of the most important parameters used to characterize two-phase flows. It is the key physical value for determining numerous other important parameters, such as the two-phase density and the two-phase viscosity, for obtaining the relative average velocity of the two phases, and is of fundamental importance in models for predicting flow pattern transitions, heat transfer and pressure drop. Some geometric definition of void fraction are outlined below;

2.6.1 The local void fraction

Various geometric definitions are used for specifying the void fraction: local, chordal, cross-sectional and volumetric, which are represented schematically in Figure 2.9. The local void fraction ε_{local} refers to that at a point (or very small volume when measured experimentally) and thus ε_{local} = 0 when liquid is present and ε_{local} = 1 when vapour is present. Typically, the local time-averaged void fraction is cited, or measured using a miniature probe, which represents the fraction of time vapour, was present at that location in the two-phase flow. If $P_k(r,t)$ represents the local instantaneous presence of vapour or not at some radius r from the channel center at time t, then $P_k(r,t)$ = 1 when vapour is present and $P_k(r,t)$ = 0 when liquid is present. Thus, the local time-averaged void fraction is defined as

$$\varepsilon_{Local}(r,t) = \frac{1}{t}\int P_k(r,t)dt \qquad 2.35$$

2.6.2 The chordal void fraction

The chordal void fraction $\varepsilon_{chordal}$ is typically measured by shining a narrow radioactive beam through a channel with a two-phase flow inside, calibrating its different absorptions by the vapour and liquid phases, and then measuring the intensity of the beam on the opposite side, from which the fractional length of the path through the channel occupied by the vapour phase can be determined. The chordal void fraction is defined as

$$\varepsilon_{chordal} = \frac{L_G}{L_G + L_L} \qquad 2.36$$

z Where L_G is the length of the line through the vapour phase and L_L is the length through the liquid phase.

The cross-sectional void fraction $\varepsilon_{c\text{-}s}$ is typically measured using either an optical means or by an indirect approach, such the electrical capacitance of a conducting liquid phase. The cross-sectional void fraction is defined as

$$\varepsilon_{c-s} = \frac{A_G}{A_G + A_L} \qquad 2.37$$

Where A_G is the area of the cross-section of the channel occupied by the vapour phase and A_L is that of the liquid phase.

2.6.3 The volumetric void fraction

The volumetric void fraction ε_{vol} is typically measured using a pair of quick-closing values installed along a channel to trap the two-phase fluid, whose respective vapour and liquid volumes are then determined. The volumetric void fraction is defined as

$$\varepsilon_{vol} = \frac{V_G}{V_G + V_L} \qquad 2.38$$

Where V_G is the volume of the channel occupied by the vapour phase and V_L is that of the liquid phase.

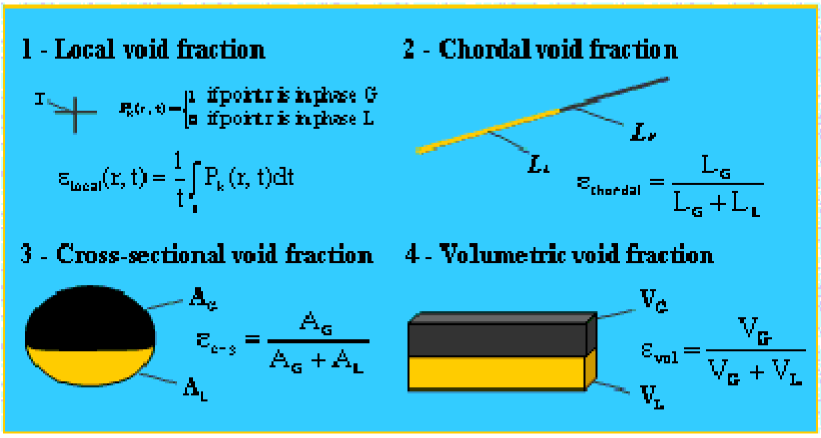

Figure 2.9: Geometrical definitions of void fraction: local (upper left), chordal (upper right), cross-sectional (lower left) and volumetric (lower right).

2.7 Radial Void Fraction Distribution

In two-phase gas–liquid flow, the local void fraction and local velocity vary across the pipe cross section. A modelling approach that takes into account this behavior is that called Drift Flux model.

Here, the main assumption is that the velocity difference is due to the drift velocity between the phases. This approach, however, relies on several empirical parameters, such as the distribution parameter Co. Analysis presented in Wallis (1969) shows that Co depends on the profiles of velocity and void fraction. As a result, efforts have been made to determine these profiles, in particular for the void fraction. In this sense, experimental measurements are of paramount importance.

The early work of Nassos and Bankoff (1967) studied the slip velocity ratios in an air–water system under steady state and transient conditions. They proposed the following equation for the radial holdup profile

$$\varepsilon_G = \bar{\varepsilon}\left(\frac{n+2}{n}\right)\left(1-\left(\frac{r}{R}\right)^n\right) \qquad 2.39$$

Where $\bar{\varepsilon}$ is the radial chordal average gas holdup along the column diameter and the exponent n are parameters and $\frac{r}{R}$ is the dimensionless radial position. The value of n is indicative of the steepness of the holdup profile. When n is large the profile is flat, for small n the profile is steep. The steepness of the holdup profile is reflected in the intensity of liquid circulation. Later, Ueyama and Miyauchi (1979) modified Eq. (2.26) as follows to include the possibility of finite gas holdup close to the wall

$$\varepsilon_G = \bar{\varepsilon}\left(\frac{n+2}{n}\right)\left(1-c\left(\frac{r}{R}\right)^n\right) \qquad 2.40$$

Where c is an additional parameter which is indicative of the value of gas holdup near the wall. If c = 1 there is zero holdup close to the wall, if c = 0 holdup is constant with changing $\frac{r}{R}$

.

More recently, Wu et al. (2001) conducted research to study radial gas holdup profiles in bubble column reactors using air and water as the operating fluids, employing gamma ray Computed Tomography (CT). (2001) used the following equation originally proposed by Luo and Svendsen (1991) for the radial holdup profile

$$\varepsilon_G = \bar{\varepsilon}\left(\frac{n+2}{n+2-2c}\right)\left(1-c\left(\frac{r}{R}\right)^n\right) \qquad 2.41$$

Wu et al. (2001) conducted correlation exercises to evaluate n and c based on the knowledge of the general operating variables and physical operating variables and physical properties of the system in order to estimate the gas holdup profile by Eq. (2.28). They concluded the following empirical relationships

$$n = 2.188\times 10^3\,\mathrm{Re}_G{}^{-0.598}\,Fr_G{}^{0.145}Mo_L{}^{-0.004} \qquad 2.42$$

$$c = 4.32\times 10^{-2}\,\mathrm{Re}_G{}^{0.2492} \qquad 2.43$$

Where

$$\mathrm{Re}_G = \frac{DU_{SG}(\rho_L-\rho_G)}{\mu_L}, Fr_G = \frac{U_{SG}{}^2}{gD}, Mo_L = \frac{g\mu_L{}^4}{(\rho_L-\rho_G)\sigma_L^3} \qquad 2.44$$

$\bar{\varepsilon}_G$, cross-sectional mean gas holdup was evaluated from the experimental data. It is against these backgrounds that the present experimental work will investigate the multiphase flow phenomena observed on the transport of air–silicone oil mixtures in a horizontal riser. Experimental studies have been conducted on a vertical 67 mm internal diameter vertical riser. A WMS was devised for air–silicone oil to measure cross-sectional void fraction and time averaged radial void fraction. The WMS is based on capacitance measurements and works with non-conductive materials such as silicone oil. Data obtained in these facilities was used for detailed analysis of phase distributions in a vertical riser in a quantitative manner.

Real time monitoring of the two-phase flow behavior using a high speed video camera was also deployed to validate the prevailing flow patterns and void fraction distribution.

2.8 Frequency

The frequency, f, is defined by Hubbard (1965), Gregory and Scott (1969) as the mean number of slugs per unit time as seen by a fixed observer. A very much used correlation for slug frequency prediction was developed by Gregory and Scott (1969) based on data by Hubbard (1965). Nydal (1991) compared the correlation with experimental data and found a good fit within the original data range (U_{SG} < 10 m/s and U_{SL} < 1.3 m/s).

$$f_s = 0.0226\left[\frac{U_{SL}}{gd}\left(\frac{19.75}{U_m}+U_m\right)\right]^{1.2} \qquad 2.45$$

Greskovich and Shrier (1972) suggested a correlation which is on the same form as the Gregory and Scott correlation. This model is presented below:

$$f_s = 0.0226\left[\frac{U_{SL}}{U_m}\left(\frac{2.02}{d}+\frac{U_m^2}{gd}\right)\right]^{1.2} \qquad 2.46$$

Manolis et al. (1995) developed a new correlation based on Gregory and Scott (1969). Taking Um,min=5 m/s and the modified Froude number

$$Fr_{\mathrm{mod}} = \frac{U_{SL}}{gd}\left[\frac{U_{m,\min}^2+U_m^2}{U_m}\right] \qquad 2.47$$

Where,

$$f_s = 0.0037 Fr_{\mathrm{mod}}^{1.8} \qquad 2.48$$

Zabaras (1999) suggested a modification to the Gregory and Scott correlation, where the influence of pipe inclination angle was included, equation (2.73). The data on which the modified correlation was tuned included positive pipe angles in the range of 0 to 11° relative to the horizontal.

$$f_s = 0.0226\left[\frac{U_{SL}}{gd}\left(\frac{19.75}{U_m} + U_m\right)\right]^{1.2}(0.836 + 2.75\sin\theta) \qquad 2.49$$

Jepson and Taylor (1993) published data from the 306 mm pipe diameter rig of the Harwell laboratory, and the effect of diameter was investigated by including 25. And 51.2 mm pipe data from Nicholson et al. (1978). A non-dimensional slug frequency was correlated against the superficial mixture velocity,

$$f_s = \frac{U_{SL}}{d}(7.59\times10^{-3}U_m + 0.01) \qquad 2.50$$

2.9 Pressure Drop

The total pressure gradient can be considered to be composed of three distinct components, that is

$$\left(\frac{dP}{dz}\right)_{TP} = \left(\frac{dP}{dz}\right)_{fric} + \left(\frac{dP}{dz}\right)_{grav} + \left(\frac{dP}{dz}\right)_{acc} \qquad 2.51$$

Where,

$\left(\frac{dP}{dz}\right)_{grav} = \frac{g}{g_c}\rho\sin\phi$ is the component due to potential energy or elevation change. It is also referred to as the hydrostatic component, as it is the only component which would apply at conditions of no flow

$\left(\frac{dP}{dz}\right)_{fric} = \frac{f\rho v^2}{2g_c d}$ is the component due to frictional loss

$\left(\frac{dP}{dz}\right)_{acc} = \frac{\rho v dv}{g_c dL}$ is the component due to kinetic energy change or convective accleration

According to the definition of flow geometry given, when the pipe is in the horizontal position, the angle and therefore the sine of the angle, are zero. This means that there is no elevation pressure drop and the pressure gradient equation becomes

$$\left(\frac{dP}{dz}\right)_{TP} = \left(\frac{dP}{dz}\right)_{fric} + \left(\frac{dP}{dz}\right)_{acc} \qquad 2.52$$

The acceleration pressure drop is usually minor and is often ignored in design calculations.

2.10 The Wire-Mesh

In order to gain insight in the measurement of cross-sectional void fraction and time averaged radial void fraction the choice was made to use a tracer with high conductivity air-silicone oil. The dispersion and mixing of this tracer in the flow is measured with a wire-mesh equipment. The wire-mesh has mainly been used as a reliable way to distinguish gasses and liquids, with high spatial and time-resolution in the cross-section of a flow. The past results in multi-phase flows, however, do not give enough information about the actual capabilities and reliability of the equipment in a single-phase environment. Therefore, the capabilities of the sensor when applied in single-phase flow is something that is looked at, as well as the possibilities of improving these capabilities.

2.10.1 An Electrode Mesh

The wire-mesh measurement technique is basically an expanded version of the conductivity measurement probe used by Taylor (1954), in his pioneering work on tracer dispersion in pipe flow. The difference is that where Taylor could measure the conductivity in one point in the flow, the wire-mesh sensor can measure the conductivity in a plane, with a spatial-resolution of millimeters and a frequency of up to 5 kHz. The wire-mesh measurement sensor was developed by Prasser et al. (1998), based on an older U.S. patent from Johnson (1987). His goal was to develop a relatively cheap measurement method with high spatial and time-resolution, able to measure gas-liquid flow distribution over the cross-section of a flow. In figure 2.14, a schematic respresentation of a wire-mesh is given. Visible are the two layers of wires, perpendicular to each other and to the flow direction, situated at a small distance from each other.

By sending small electronic pulses one by one through each of the transmitter wires and measuring the received signal in every receiver wire separately, the conductivity of the fluid at every separate crossing between two wires is measured.

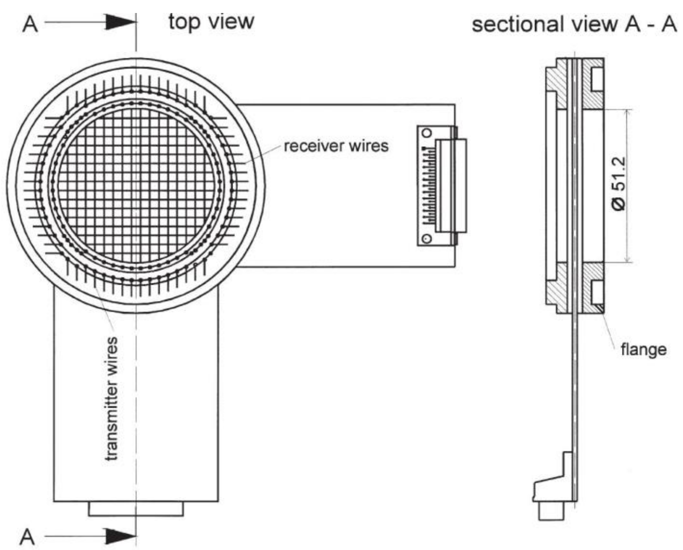

Figure 2.10: **A schematic respresentation of a wire-mesh sensor by Prasser et al. (1998).**

2.10.2 The Measurement Principle

The measurement principle of the wire-mesh sensor itself rests on a simple principle. It measures the conductivity of two wires which are separated by a small distance filled with the fluid that is to be measured which in this case is air-silicone oil. It manages to create a lot of measurement points in a plane by using a multitude of wires, which are controlled by some electronic equipment that also processes the acquired data.

2.10.3 The Sensor

The wire-mesh sensor that is used in this project is capable of measuring the conductivity of multiple points in a plane. Wire-mesh sensors based on capacity measurements are also available but will not be used in this research. In figure 2.15, a schematic of the wire-mesh system from the original paper by Prasser et al. is shown. It consists of four wires in one plane, through which electrical pulses are transmitted, and four wires located at a small distance below the top plane (2 mm in Prasser's case) perpendicular to the transmitter wires. The planes of the wires are perpendicular to the direction of the flow, so, when looking in the flow direction, every transmitter wire has one 'cross-point' with each receiver wire. Since the transmitter wires are transmitting a pulse one by one, the conductivity of the fluid flowing through one of the crossings in the mesh can be acquired by measuring the signal that is transmitted through the fluid from the transmitting wire to the receiving wire. In this example, this results in sixteen effective conductivity-measurement points in the measurement plane.

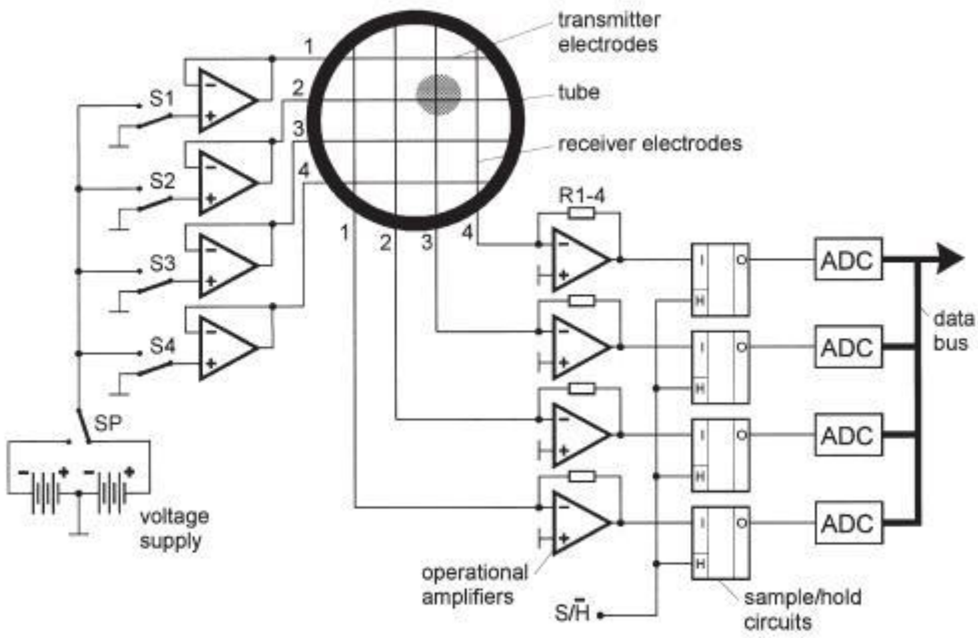

Figure 2.11: The wire-mesh sensor as it was designed by Prasser et al. (1998).

2.10.4 The Electronics

In order to prevent electrolysis the pulses that are transmitted are not DC, but consist of alternating positive and negative signals of equal size. Also, when a conductive fluid is present the received signal shows transient behavior because of the capacitance of the wires. In order to minimise this effect, the actual moment of measuring the received signal is after the transient behavior has died out, as can be seen in figure 2.16. Another problem with this setup, that Prasser et al. managed to solve with their design, is the surpression of cross-talk. For a sharp resolution, it is vital that only the wire with a driven current is transmitting a signal. However, since the transmitter wires can be close to each other it is necessary to prevent the electrical field from the transmitting wire to generate a signal in neighboring wires. This cross-talk would result in a blurring of the signal, which is undesirable. In order to prevent this, the wire-mesh is constructed such that the wires have a significantly lower impedance than the fluid between them. This way, there is no driving potential difference between wires, so cross-talk is effectively surpressed (Prasser et al., 1998).

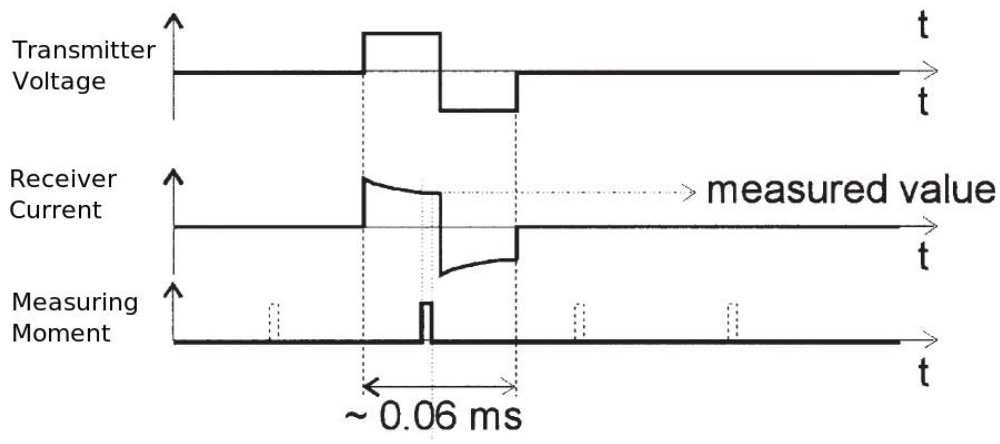

Figure 2.12: **The transmitted and received signal, and the moment of measuring, from Prasser et al. (1998).**

2.10.5 Multi-Phase Flows

Since its invention, the wire-mesh has been used both at Delft University and in other places in various experiments and geometries for different purposes. Examples of wire-mesh-based research in Delft are Manera (2003), Belt (2007), Smeets (2009) and Descamps (2007), who performed measurements with a wire-mesh for different purposes. Manera looked at the flashing induced instabilities in the gas-liquid flow when starting a BWR, Belt used a novel custom-designed wire-mesh for measuring the film-thickness at the walls in annular flow, and Descamps measured the bubble sizes in a gas-driven driven vertical flow. Outside Delft, the the wire-mesh technology has been used in a similar range of applications, with Prasser et al. (2005) comparing the capabilities of a wire-mesh with fast X-ray tomography, Pietruske and Prasser (2005) using the apparatus for measurements in high flow and pressure multi-phase flow, and Silva et al. (2007) developing a wire-mesh that uses the capacitance of a fluid instead of its conductivity. In figure 2.17 an example of a wiremesh used in a two-phase flow by Prasser et al. (2005) is shown. The signal output of the wire-mesh is not dependent on the fluid properties at the crossing of two wires but actually it depends on the mean properties at of the fluid in a small volume between the two wires. Because of this, the output can vary depending on how big a piece of this volume is covered by a bubble. This makes it possible to use the wire-mesh for the reconstruction of bubble sizes and shapes, as well as the measuring of void fractions, as done by Prasser et al. (2005).

Figure 2.13: The measurement of a gas bubble with a wire-mesh in a two-phase flow Prasser et al. (2005)

CHAPTER 3
EXPERIMENTAL DESIGN

3.0 Experimental Arrangements

The analyses performed on experimental laboratory data provide the main source of information about specific multiphase flow regimes. This chapter presents a summary of the results obtained from a series of two-phase air-silicone oil flow laboratory experiments that were performed on an inclinable pipe flow rig which is available within the L3 Laboratories of the Department of Chemical and Environmental Engineering at the University of Nottingham. This chapter presents a detailed description of the experimental rig used to study the flow behaviour present in horizontal and horizontal orientated 0° bends. An overview of the experimental facility and the choice of test fluids are given in Sections 3.1 and 3.2, respectively. Furthermore, Sections 3.4 provide the methodology used during the experiments.

3.1 Overview of the Experimental Facility

The first series of experiments were performed on an inclinable pipe flow rig, shown in Figure 3.1. This rig had previously been employed in multiphase annular flow studies executed by Azzopardi et al. (1997), Geraci et al. (2007a), Geraci et al. (2007b) and more recently for the study of bubbly, slug and churn flow by Hernandez-Perez (2008). The experimental facility consists of a main pipe flow test section made from transparent acrylic pipes of 0.067 m inside diameter and 6 m long to allow for the development of the injected flow over the length of the test section. The test section is constructed from a series of conjoined short sections of pipe with a flange joint at either end. Each of these smaller test sections may be easily installed or replaced, to lengthen or shorten the length of the test section. The rigid steel frame supporting the test pipe section is constructed to enable the test pipe section to be inclined at angles of from -5 o to 0° to the horizontal. This enables the researcher to investigate the influence that different inclinations may have on the flow patterns generated. The experimental rig was charged with an air/silicone oil mixture. The experiments were all performed at an ambient laboratory temperature of approximately 20°C. The physical properties of the fluids used in the experiments are as shown on Table 3.1.

Figure 3.1: Picture of the inclinable rig.

3.2 System (Test Fluid)

The air-silicone oil system was selected for several reasons:

- Thermal stability and transfer qualities - at both hot and cold extremes
- Electrical insulation
- Fire resistance
- No toxicity, which makes it environmentally safe, and reasonable in cost
- No odour, taste or chemical transference
- Easily discernable in acrylic pipe

- Several proven techniques including the advanced instrumentation exist for liquid holdup and/or void fraction measurements for silicone oil.

The properties of the two fluids used in the experiments are shown in Table 3.1.

Table 3.1: Properties of the fluids at 1 bar at 20°C

Fluid	Density (kgm^{-3})	Viscosity $(kgm^{-1}s^{-1})$	Surface Tension (Nm^{-1})	Thermal conductivity $(Wm^{-1}K^{-1})$
Air	1.18	0.000018	0.02	0.1
Silicone Oil	00	0.00525		

3.3 Description of Flow Facility

The flow facility consists of a liquid storage tank, liquid centrifugal pump, compressed air line, liquid and air rotameters, and a cyclone (separator). A horizontal
0° bend with a radius of curvature 154 mm was attached to the top of the pipe flow test section of the rig (Figures 3.2 and 3.3) to enable the effects that a 0° bend connected in series may have on air-silicone oil around the bend section. At the top of the pipe flow test section before the bend, WMS measurement transducers were installed at different axial positions (dimensionless axial distances from mixer are 66, 67 and 73 pipe diameters). Data provided by these transducers will allow for the measurement of the time varying liquid holdup and the void fraction, respectively. It should be noted that it was not possible to mount the WMS upstream of the ECT sensor, since a visual examination concluded that the intrusive wire mesh of the WMS changed the nature of the flow completely by breaking up large bubbles and temporarily homogenising the flow immediately downstream of the device. The large bubbles were observed to re-form within approximately one pipe diameter.

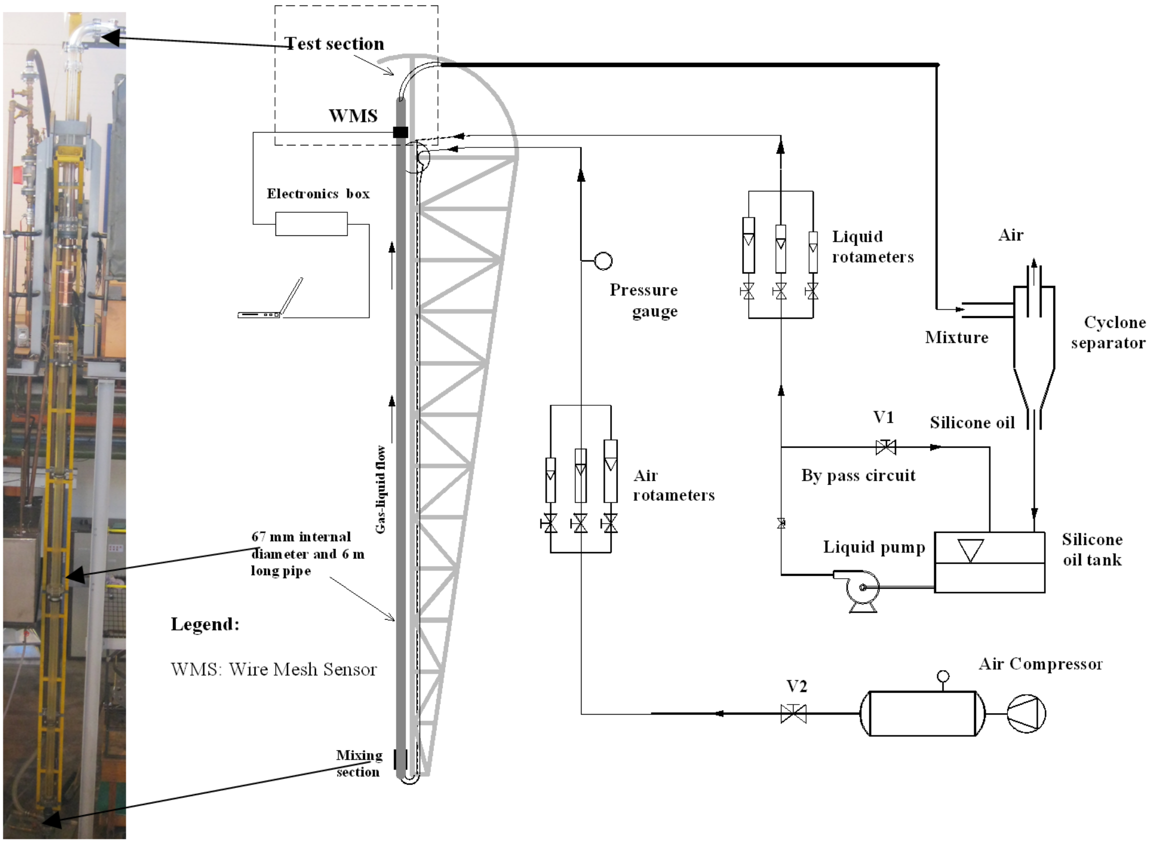

Figure 3.2: Diagram showing the inclinable rig converted to a horizontal 0° bend. The left hand side of the figure shows the actual picture of the rig.

3.4 Wire Mesh Sensor

Local time varying void fractions were obtained by using the WMS measurement transducer developed by Presser et al. (1998 and 2001). The sensor shown in Figure 3.11 consists of two parallel wire grids positioned orthogonally but offset by a small distance in the axial direction. One grid works as a transmitter while the other as a receiver. By activating each wire successively, the current at each crossing point is detected. The local instantaneous void fractions are calculated from the measured capacitance between crossing points, a series of 2 dimensional data sets can be obtained. By reconstructing these sets in time sequence a high speed visualization may be achieved.

In this study, a 24 × 24 wire configureuration sensor was used that had been previously applied for conductivity measurements. The sensor comprises two planes of 24 stainless steel wires of 0.12 mm diameter, 2.8 mm wire separation within each plane, and 2 mm axial plane distance. The wires are evenly distributed over the circular pipe cross-section. Since the square sensor is installed in a circular pipe, only 440 of the total 576 wire crossing points are within the radius of the pipe. The spatial resolution of the images generated by the sensor is 2.8 mm, which corresponds to the wire separation within a single plane. Data was acquired at a frequency of 1000 Hz for a 60 second experimental run period. An acrylic frame supports the sensor and allows fixation into the text flow pipe section. Figure 3.10 shows a photograph of the sensor.

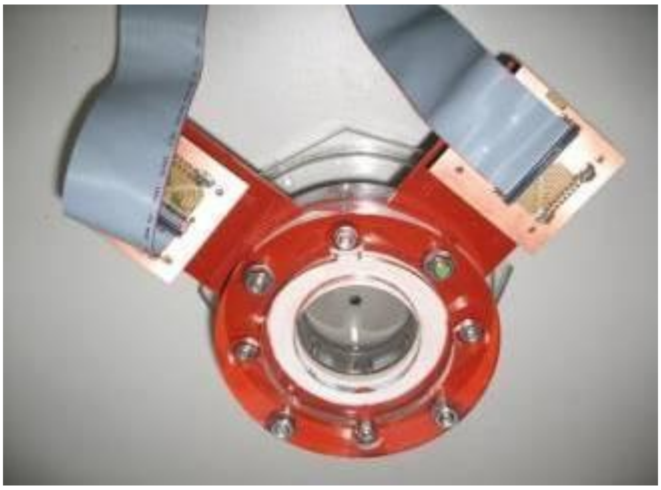

Figure 3.3: Wire mesh sensor (WMS)

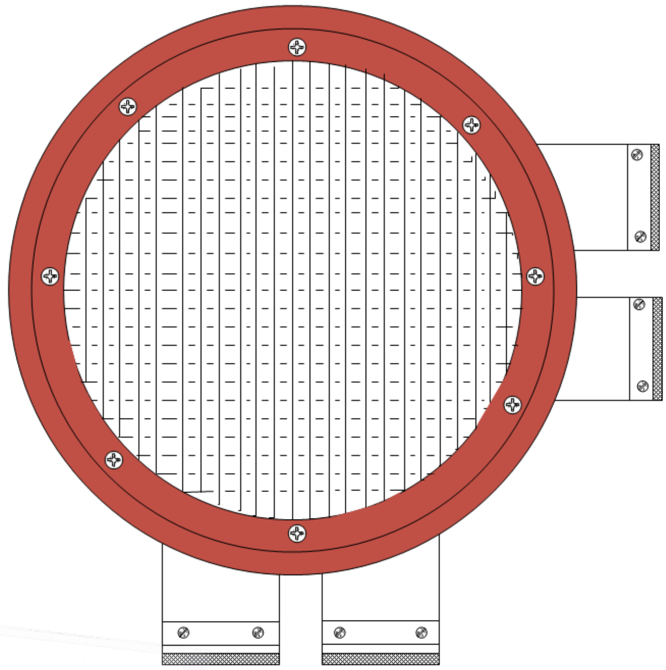

Figure 3.4: 24 × 24 wire mesh sensor for pipe flow measurement

3.5 Processing of Void fraction profiles

Radial time averaged void fraction were calculated by averaging the local instantaneous void fractions over the measurement period and over a number of ring-shaped domains (m). This is done by the following equation:

$$\bar{\varepsilon} = \frac{1}{k_{\max}} \sum_{k} \sum_{i} \sum_{j} a_{i,j,m} . \varepsilon_{i,j,k} \qquad \text{Eq. 1}$$

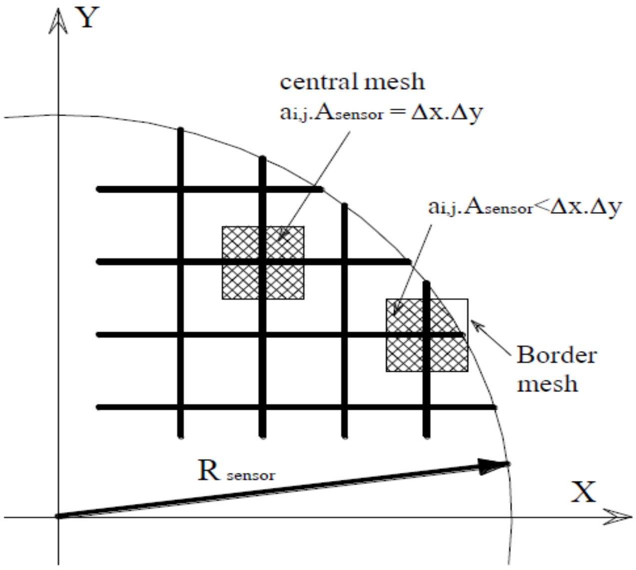

Figure 3.5: Weight coefficients for the cross-section averaging of local void fractions measured by the WMS (Prasser et al. (2002))

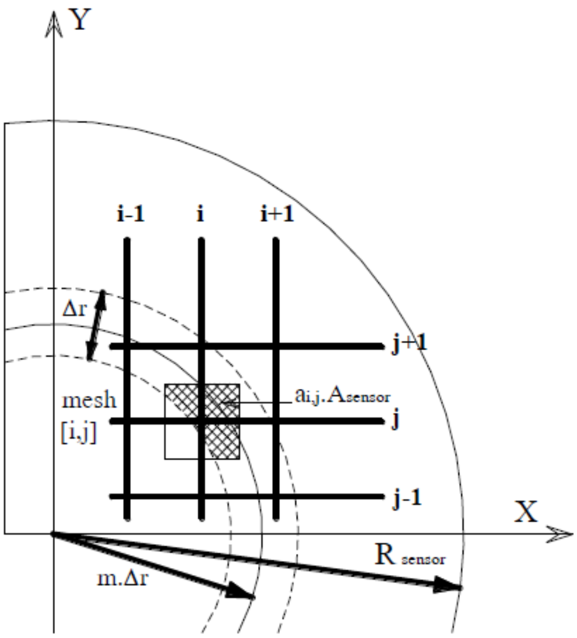

Figure 3.6: Weights coefficients for the cross-section averaging of local void fractions over a number of ring-shaped domains (Prasser et al. (2002))

CHAPTER 4
RESULTS AND DISCUSSION

4.0 Introduction

This section presents a comparison of the mean void fraction distribution obtained over a range of different gas superficial velocities. It will also compare the radial time averaged void fraction (%) for all cross points (24×24 values) of the WMS from axis of pipe in (mm). The probability density functions (PDF) of void fraction are also presented. Performance analysis of the void fraction correlations was also made. The effect of gas superficial velocity on flow patterns, radial time averaged void fractions and the variation of time averaged cross-sectional void fraction distribution were also analyzed. The pressure drop analysis is also made and the experimental frequency was also compared with empirical models.

4.1 Flow Pattern Map

Flow patterns have an important influence on prediction of the void fraction, flow boiling and convective condensation heat transfer coefficients, and two-phase pressure drops. The prediction of flow pattern transitions and their integration into a flow pattern map for general use is thus of particular importance to the understanding of two-phase flow phenomena and design of two-phase equipment. For these reasons it is therefore absolutely necessary to specify as precisely as possible the features of the flow used to characterize the pattern designated. When a gas-liquid mixture flows along a deviated pipe, the mixture can arrange itself in different geometric distribution of the phases, influenced by several variables such as inlet flow rates, pipe geometry, and orientation of flow and fluid properties. These geometric configureurations are usually referred to as flow pattern or regimes. The flow pattern map has been an effective tool of identifying which flow regime occurs for a given set of flow rates.

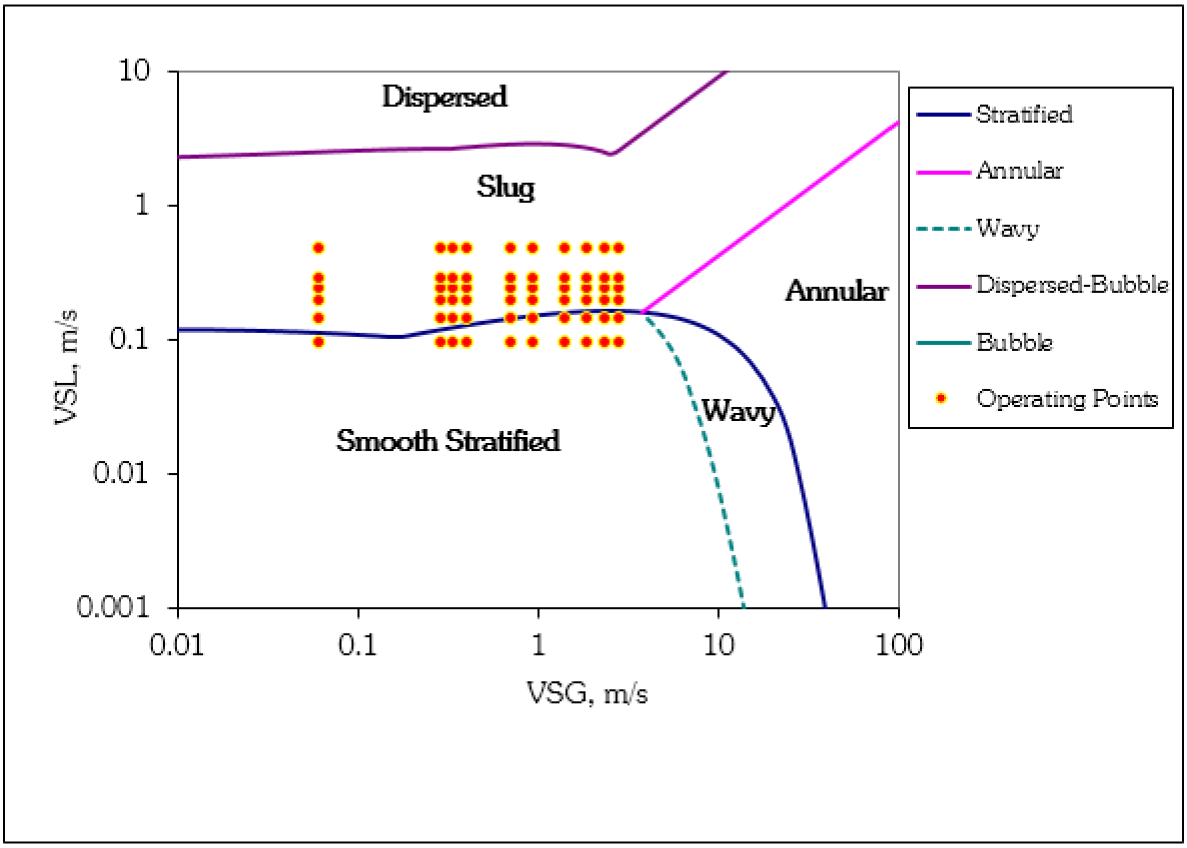

Figure 4.1: **(Shoham, 2006)'s flow pattern map for experimental data (Text Matrix)**

(Shoham, 2006)'s flow pattern map was adopted in this work to determine the flow pattern transitions of the experimental data. In order to achieve excellent results, the flow pattern map requires an input data and such required data include; fluid properties, pipe geometry; and the operating points which include: both gas and liquid superficial velocities.

From figure 4.1, it can be observed that the expected flow patterns are partly smooth stratified (SS) flow and slug (SL) flow and the dominant flow regime is slug as expected for horizontal fluid flow under such conditions. Critical observation also indicates that liquid superficial velocity of 0.142 m/s and corresponding gas superficial velocities of 0.709 and 0.945 m/s lie in-between slug and smooth stratified flow, hence no clear flow regime.

4.2 Performance analysis of the void fraction correlations

In the literature numerous correlations are available to predict the void fraction in horizontal two phase. The performance analysis of these available correlations was necessary because most of these correlations developed by different investigators were based on the data limited in number, pipe diameter, flow pattern, fluid combinations and system pressure. It is therefore imperative to mention here that by nature all the empirical correlations have some sort of limitations, even though not explicitly reported by their authors. This is due to the very fact that they were fitted to given data sets which in turn depend on the inherent physical limitations of the experiment under which the data was collected. The empirical correlations are classified into four categories by Vijayan et al. (2000). These are Slip ratio correlations, $K\alpha_H$ correlations, Drift flux correlations and General void fraction correlations. These various categories are explained in detail in chapter 2. The empirical correlations considered here falls under Drift flux correlations category. This type of correlations are based on the work of Zuber and Findlay (1965) where the void fraction can be predicted taking into consideration the non-uniformity in flows and the difference in velocity between the two phases (liquid and gas).

In this section, the accuracy and performance of the empirical correlation would be ascertained by means of percentage error and Root Mean Square (RMS) error in order to select the best. The inherent limitations in the various correlations have called for these modes of analysis. The empirical correlations which were considered are Clark and Flemmer (1985), Cai et al. (1997), Greskovich and Cooper (1975) Hassan (1995), Kokal and Stanislav (1989), Bankoff (1960), Zuber-Findlay (1965) Ahmad (1964), Nicklin et al. (1962) and Hughmark (1962).

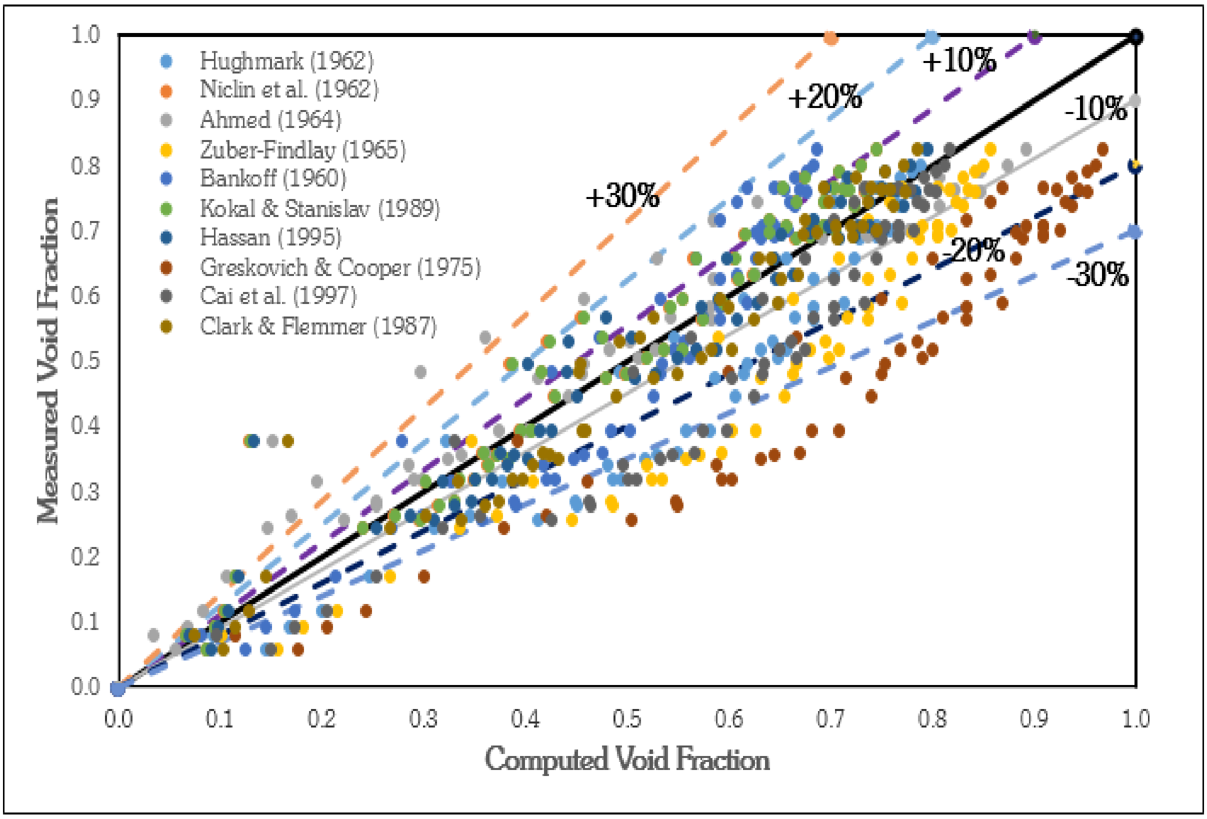

Figure 4.2: Comparison by percentage error of void fraction obtained using the WMS (present study) with empirical correlations.

Table 4.1 Best correlation based on RMS error in descending order

Emperical Correlation	RMS Error (%)
Nicklin et al.(1962)	16
Kokal& stanislav (1989)	16
Hassan (1995)	16
Clark & Flemmer (1987)	20
Ahmad (1964)	20
Bankoff (1960)	28
Hughmark (1962)	40
Cai et al. (1997)	43
Zuber-Findlay (1965)	49
Greskovich & Cooper (1975)	65

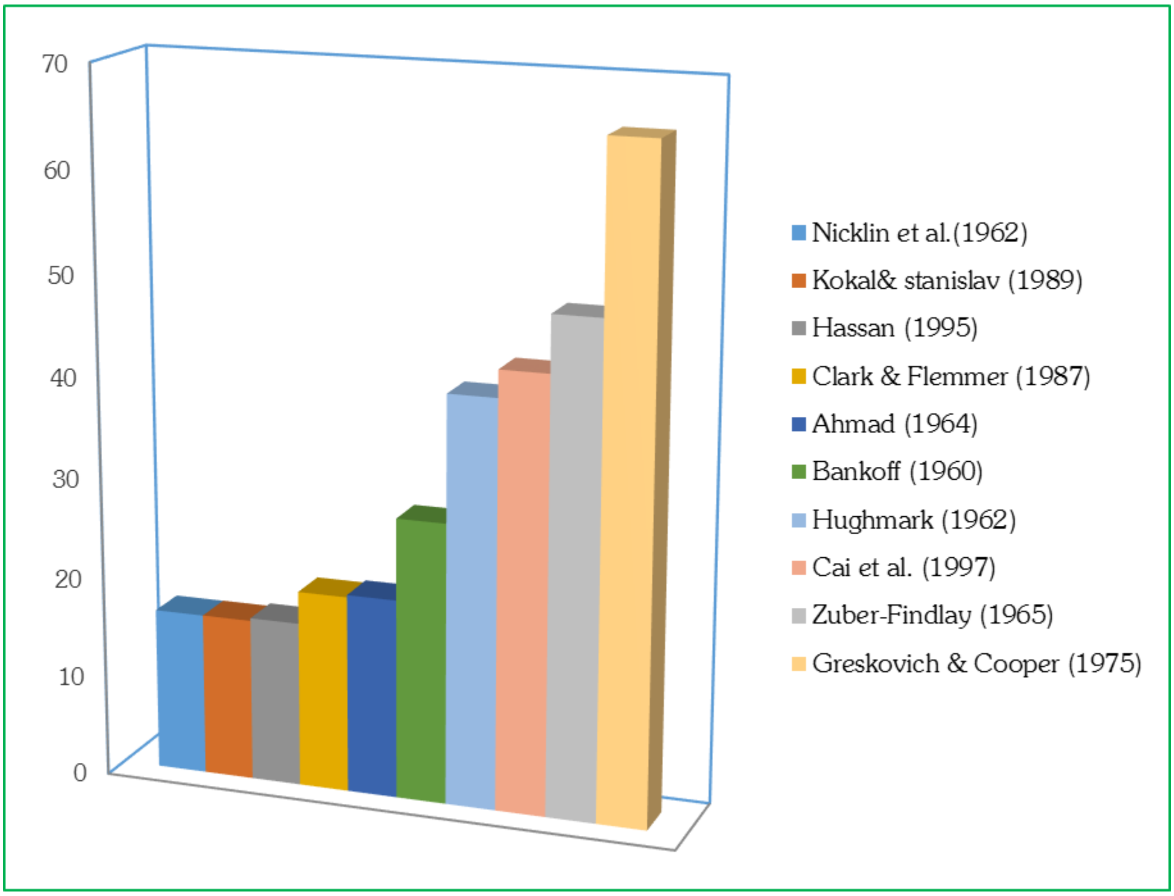

Figure 4.3: **Root Mean Square (RMS) error of average void fraction from empirical correlations**

$$RMS = \sqrt{\left[\frac{1}{N-1}\sum_{i=1}^{N}\left(\frac{\alpha_{predicted} - \alpha_{measured}}{\alpha_{measured}}\right)^2\right]} \times 100\% \qquad \text{Eq. 4.1}$$

From figure 4.3 it can also be observed that based on the RMS error discrimination which was computed from Eq. 4.1 and the results tabulated in Table 4.1 and also shown graphically with the aid of a 3-D clustered column in figure 4.3, Nicklin et al. (1962), Hassan (1995) and Kokal and Stanislav (1989) had the least error of hence adjudged to be the best correlations relative to the others. This finding amazingly confirmed that which was based on the percentage error and therefore can be concluded that these three correlations are just the best so far as these two different analyses are concerned. Greskovich and Cooper (1975) once again was adjudged to be the least performing correlation and obviously should not be adopted because it has error margin.

From figure 4.2, it can be observed that based on the percentage error discrimination, Hassan (1995) was concluded to be the best empirical correlation with $\pm 10\%$ deviation. Even though Hassan was judged to be the best, Kokal and Stanislav (1989) and Nicklin et al. (1962) were also observed to have $\pm 10\%$ deviation but had few points within $\pm 15\%$ deviation but can still be concluded to have good accuracies. Hence, Hassan (1995), Kokal and Stanislav (1989) and Nicklin et al. (1962) could be chosen when considering horizontal two phase flow because it would have better performance relative to other correlations and also agree more with the experimental data. However, based on this analysis, Greskovich and Cooper (1975) should not be selected so far as horizontal two phase flow is concerned because it has over $\pm 30\%$ deviation from the experimental data and would not do any good should it be chosen.

4.3 Variation of time averaged cross-sectional void fraction distribution with gas superficial velocity

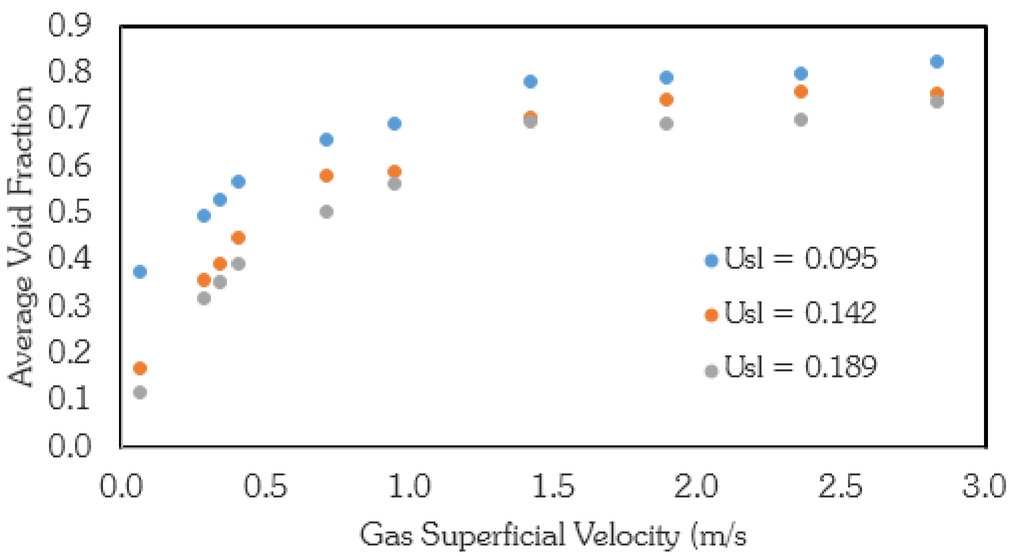

Figure 4.4: **Variation of time averaged cross-sectional void fraction with gas superficial velocity for different liquid superficial velocities of 0.095 < U_{SL} < 0.189 m/s**

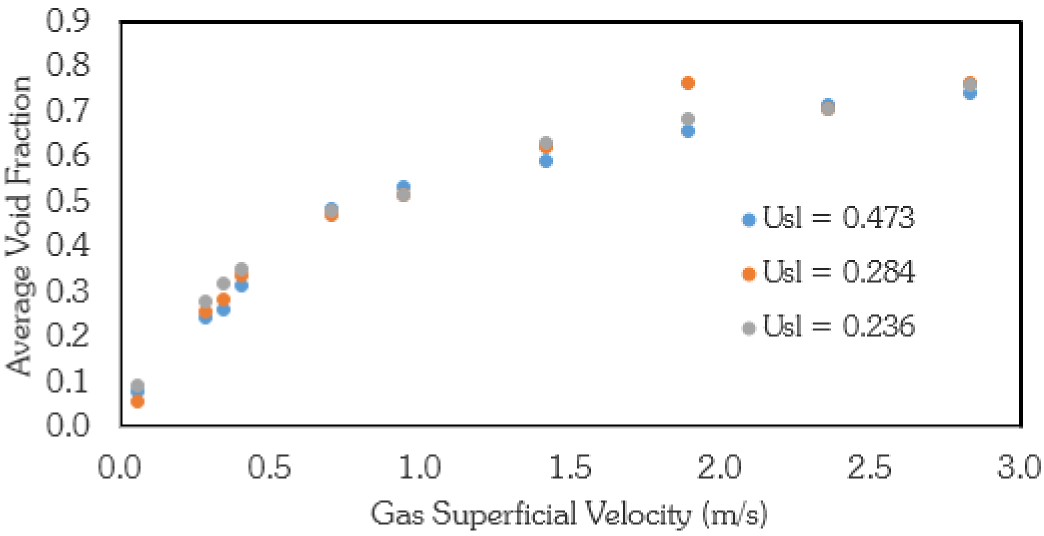

Figure 4.5: **Variation of time averaged cross-sectional void fraction with gas superficial velocity for different liquid superficial velocities of (a) 0.236 < USL < 0.473 m/s**

From figures 4.4 and 4.5 which show plots of average void fraction against gas superficial velocity, it can be observed that at constant liquid superficial velocity, the average void fraction increases with an increase in the gas superficial velocity. However, the average void fraction increases with a decrease in liquid superficial velocity. This observed trend in void fraction is in agreement with the observations of Abdulkadir et al. (2014) and Abdulkadir et al. (2010). It can also be observed from the plot that for a liquid superficial velocity of 0.095 m/s, the average void fraction, started initially with 0.378 at a gas superficial velocity of 0.047 m/s and extended to a maximum value of 0.78 at a gas superficial velocity of 4.727 m/s. It also shows that for liquid superficial velocities of 0.142, 0.189 and 0.236 m/s, the initial average void fraction is 0.1 at a gas superficial velocity of 0.047 m/s and reached average void fraction of 0.80, 0.77 and 0.74 respectively at a gas superficial velocity of 4.727 m/s. For further liquid superficial velocities of 0.28 and 0.473 m/s, a maximum average void fraction of 0.75 and 0.75 respectively is obtained at both gas superficial velocities of 4.727 m/s and starting initially with an average void fraction of 0.1 at a gas superficial velocity of 0.047 m/s.

4.4 Wu et al. (2001)'s published equation compared to the experimental time averaged radial void fraction

Wu et al. (2001) recently conducted a research to study radial gas holdup profiles in bubble column reactors using air and water as the operating fluids, employing gamma ray Computed Tomography (CT). They used equation 4.2 which was originally proposed by Luo and Svendsen for the radial holdup profile. The analysis which was done here was to examine whether Wu et al. (2001)'s equation which was mainly to study bubble column reactors can fully predict or replicate the observed radial void fraction in horizontal orientation.

$$\varepsilon_G = \bar{\varepsilon}\left(\frac{n+2}{n+2-2c}\right)\left(1-c\left(\frac{r}{R}\right)^n\right) \qquad \text{Eq. 4.2}$$

From an examination of the experimental data plotted in Figure4.6, it can be observed that the radial void fraction increases with gas superficial velocity and that the shape of the profile is dependent on the gas superficial velocity. It is interesting to note that Wu et al.'s equation which was not meant for analysis in horizontal orientation was able to replicate almost exactly the observed radial void fraction in the horizontal orientation considered in this work. It can also be observed that even at low and high gas superficial velocity the model was able to replicate the respective trends which are contrary to the findings made by Abdulkadir et al. (2014). In their study they found out that the comparison between the experimental data and Wu et al.'s equation was very poor at low liquid and gas superficial velocity but could better replicate at higher gas superficial velocity. In conclusion, even though Wu et al.'s model was proposed for vertical orientation with air and water used as the operating fluid, it could as well replicate the observed radial void fraction in the horizontal orientation even with air and silicone oil used as the operating fluid.

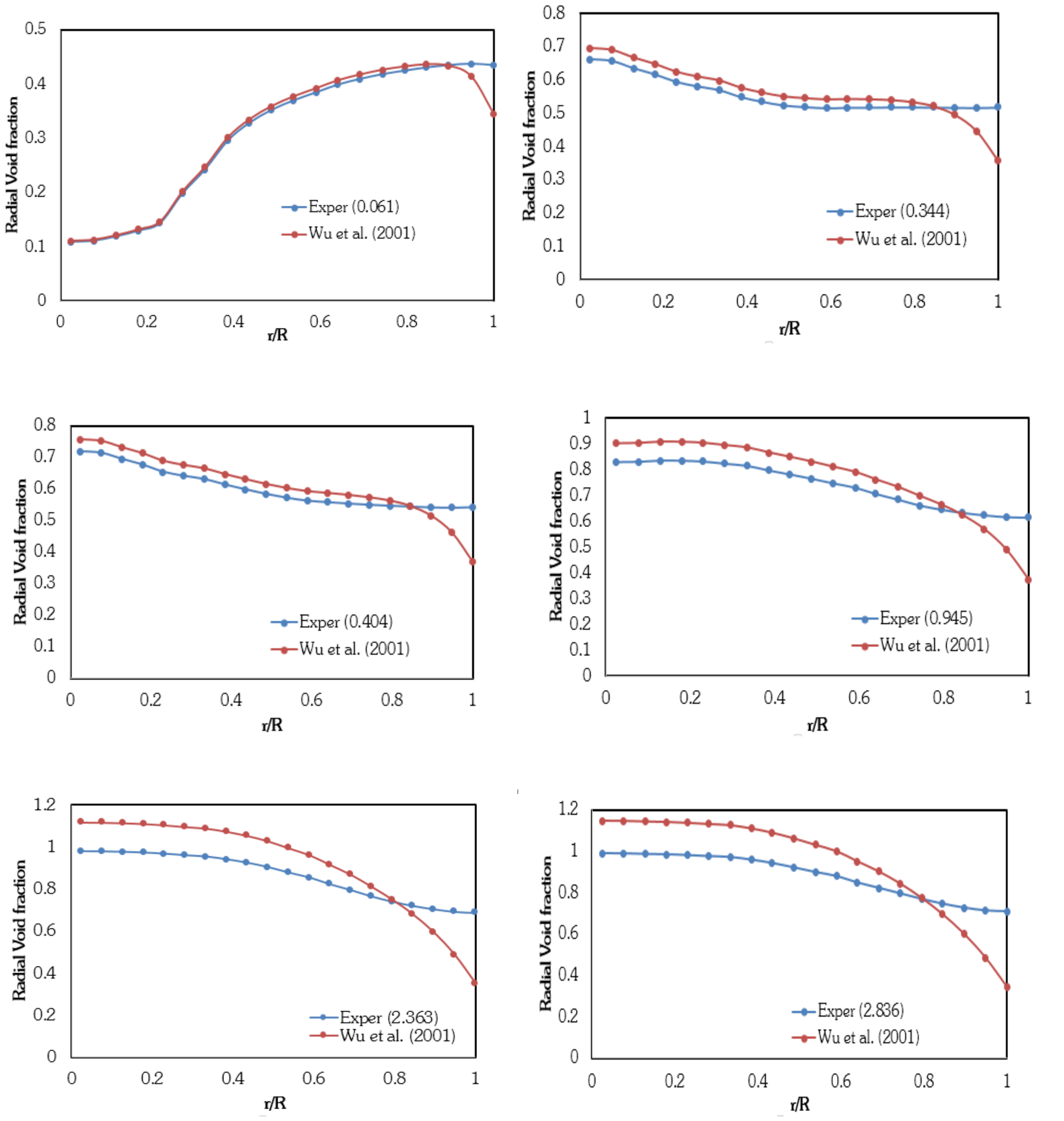

Figure 4.6: Comparison of experimental time averaged radial void fraction distribution with Wu et al. (2001)'s published equation at liquid and gas superficial velocities of 0.095 m/s and ($0.061 \leq U_{SG} \leq 2.84$ m/s), respectively. The Wu et al.'s published equation was recalculated using air and silicone oil physical properties.

4.5 The effect of gas superficial velocity on flow pattern and radial void fraction profile

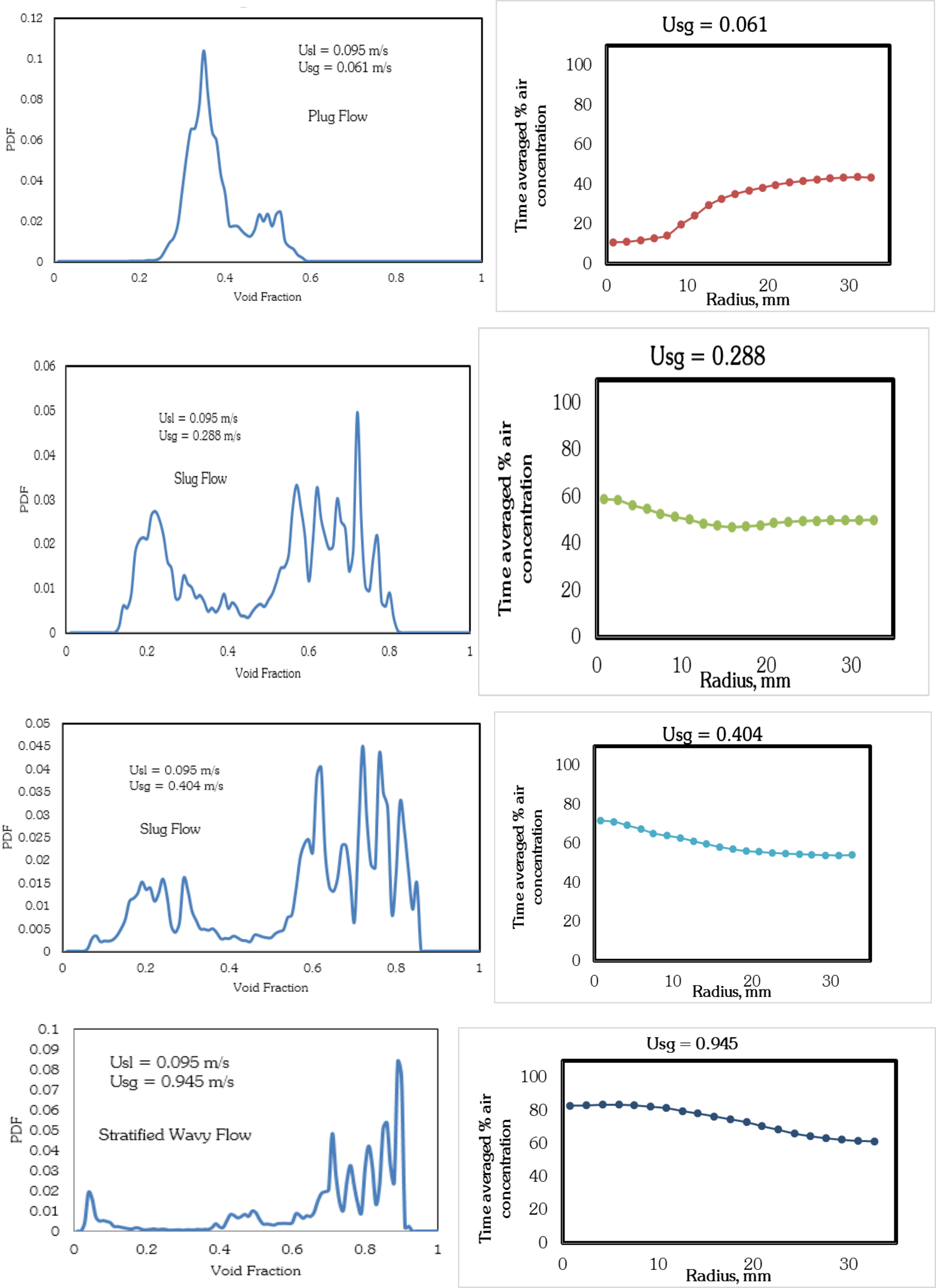

Figure 4.7a: The effect of gas superficial velocity on flow pattern and radial void fraction profile.

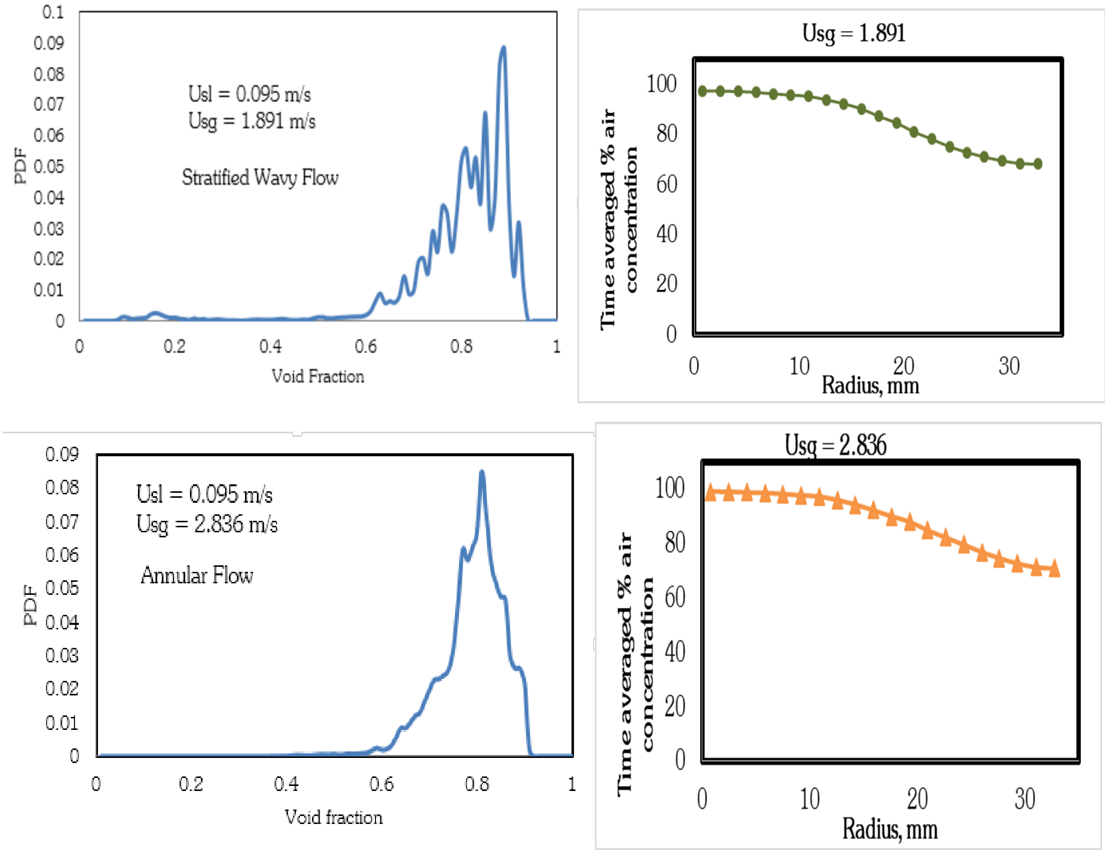

Figure 4.7b: **The effect of gas superficial velocity on flow pattern and radial void fraction profile. The maximum and minimum % radial void fraction occurring at 0.8 and 32.7 mm respectively.**

It can be observed from Figure 4.7 that at liquid and gas superficial velocities of 0.095m/s and 0.061 < USG < 2.84 m/s, respectively, cubic profiles are obtained. The profiles show that maximum and minimum radial void fractions are observed at the center of the pipe and pipe wall respectively. The maximum radial void fractions for the six profiles as observed from the figure are 43.4 %, 59.0 %, 71.8 %, 83.0 %, 97.2 %, and 99.1 %, respectively. The profiles then moved downwards and then moved slightly upward where it remained at a constant minimum. The minimum radial void fractions so obtained are 10.9 %, 50.1 %, 54.2 %, 61.5 %, 68.07 % and 70.8 %, respectively. The maximum and minimum percentage radial void fractions occurred at 0.8 and 32.7 mm, respectively with the exception of gas superficial volocity of 0.061 m/s which had the minimum and the maximum percentage radial void fraction occuring at 0.8 and 32.7 mm respectively. It can also be obseved that, unlike the other flow conditions where the profile moved downward and then slightly upward at a constant miminum, Usg of 0.061 m/s had the profile moving upward and then moving slightly downward at a contant minimum.

The cubic profiles obtained in this present study are contrary to the results reported by (Abdulkadir et al., 2014), (Abdulkadir et al., 2010) and (Ohnuki and Akimoto, 2000) which is expected because the experimental studies of (Abdulkadir et al., 2014) and (Abdulkadir et al., 2010) were developed along a vertical pipe with a flow condition of air/silocone and that of (Ohnuki and Akimoto, 2000) with air/water. The results therefore, show that an increase in gas superficial velocity greatly owes for an increase in radial void fraction at the center of the pipe and pipe wall. It can also be be obseved from the PSD plot that at low superficial gas velocity, plug flow regime was experienced and as the gas superficial velocity increased the flow regime transited to slug flow and to stratified flow with further increase in gas superficial velocity and then ended with annular flow with further increase. These flow regimes experienced are in agreement with flow patterns associated with horizontal pipes as expoused in literature. The results also show that the flow reqimes, the shape of the radial void fraction profile and an increase in percentage void fraction are dependent on gas superficial velocity as shown in Figure 4.7.

4.6 Pressure Drop Analyses

One important paramater that cannot be left out when it comes to pipeline design is pressure drop. The pressure drop in a system is an essential variable for the determination of the pumping energy for a given flow. The diversity of techniques used by different authors to present the two-phase flow pressure drop Baker, (1957), Griffith and Wallis (1961), Bonnecaze et al. (1971), Grescovich and Shrier (1971), Chen and Spedding (1981) and Jepson and Taylor (1993), indicates among other things that pressure drop in two-phase flow can depend on a significant number of variables such as mass flow rate, which reduces with increasing void fraction; inclusion-induced wall shear, which increases with void-fraction where the conduit diameter is also very important. The effect of gravity on the pressure drop is very obvious in that, when the fluid flow against gravity the pressure drop is very high and the converse is also true.

In this work, Beggs and Brill (1973) correlation was used to ascertain the pressure drop and results onbtained are presented in figures 4.8, 4.9, 4.10 and 4.11. Critical observation from these aforementioned figures clearly indicates that for horizontal flow, the main contributor for the total pressure drop is the frictional shear stress which is dependent on the mixture density, which in turn is a function of the in-situ volume fraction or liquid hold up. This fact is proved by the experimental results in figures presented below.

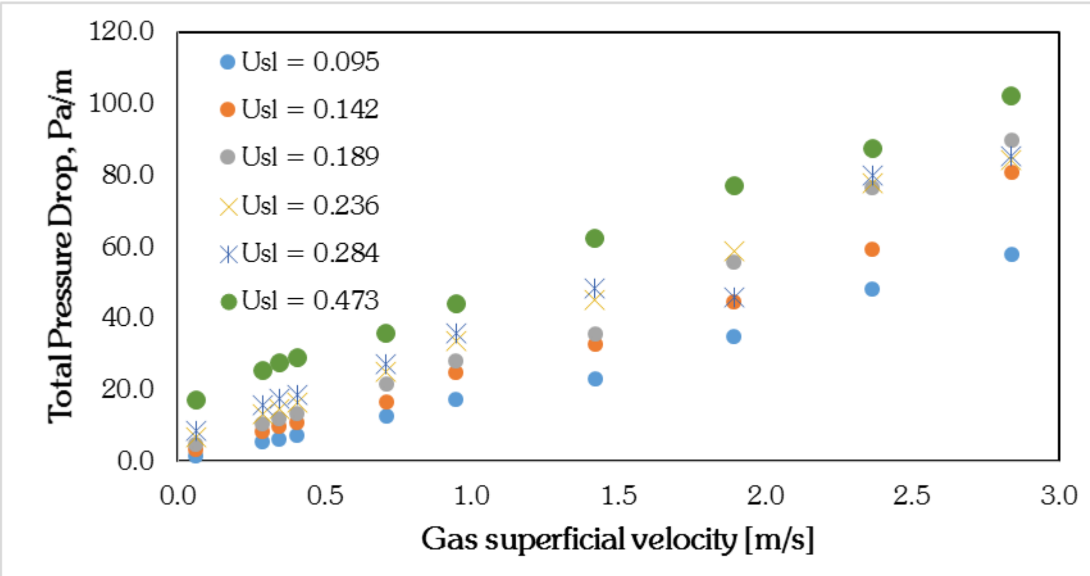

(a)

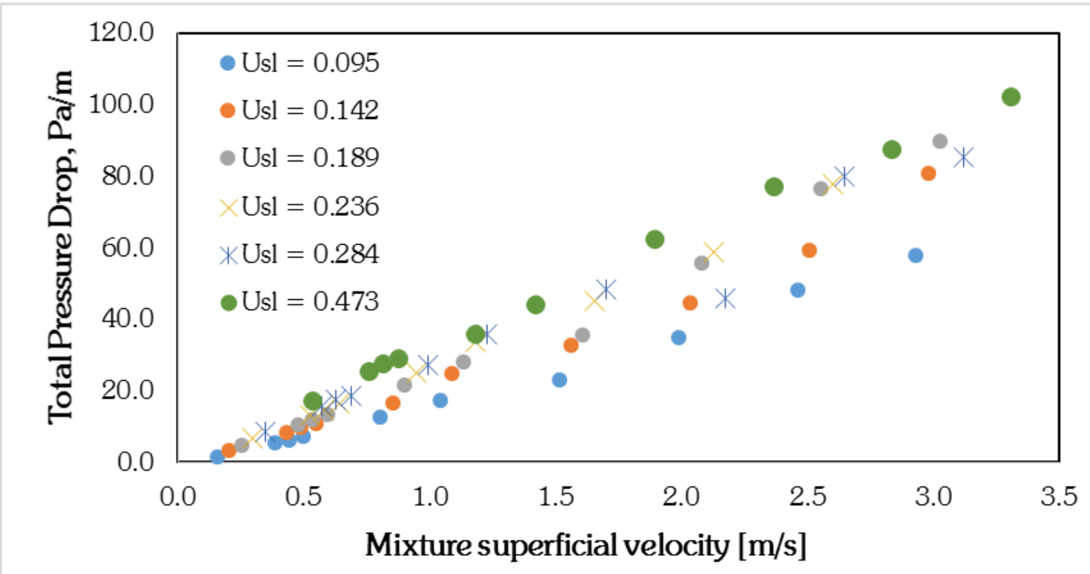

(b)

Figure 4.8: Influence of gas and mixture superficial velocities on the total pressure drop at varying liquid superficial velocities

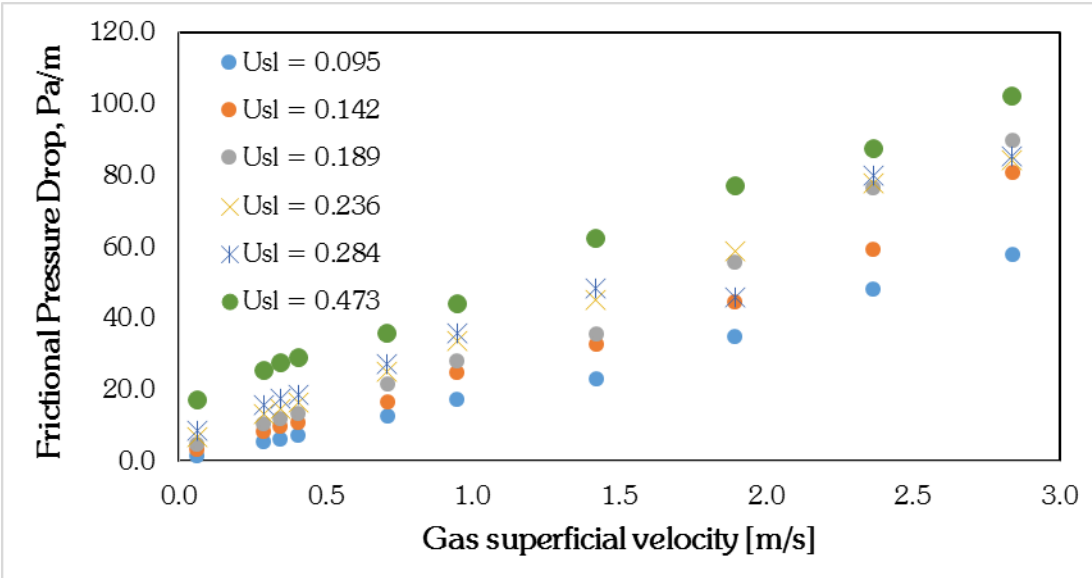

(a)

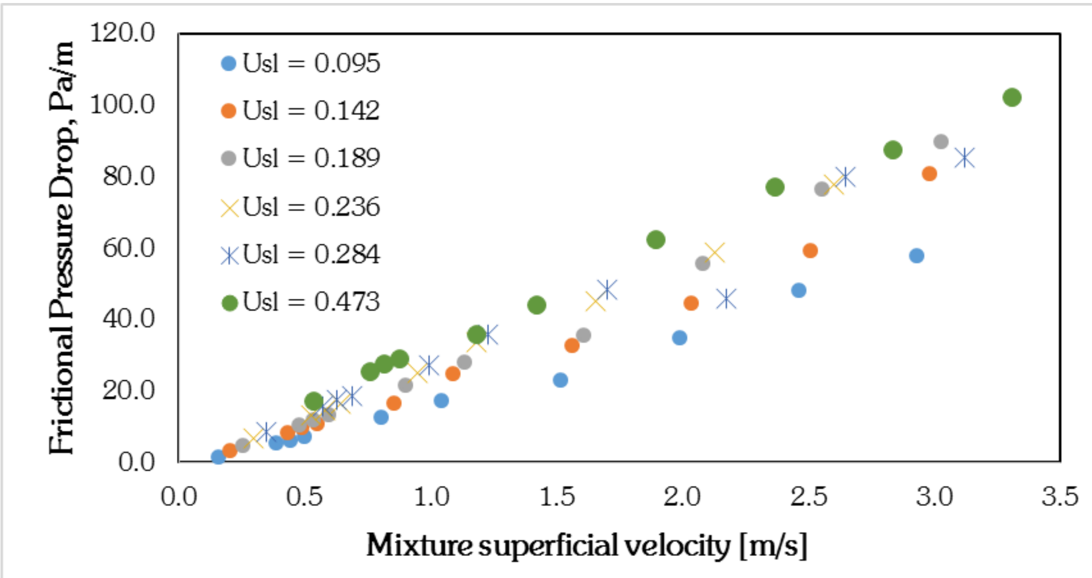

(b)

Figure 4.9: Influence of gas and mixture superficial velocities on the frictional pressure drop at varying liquid superficial velocities

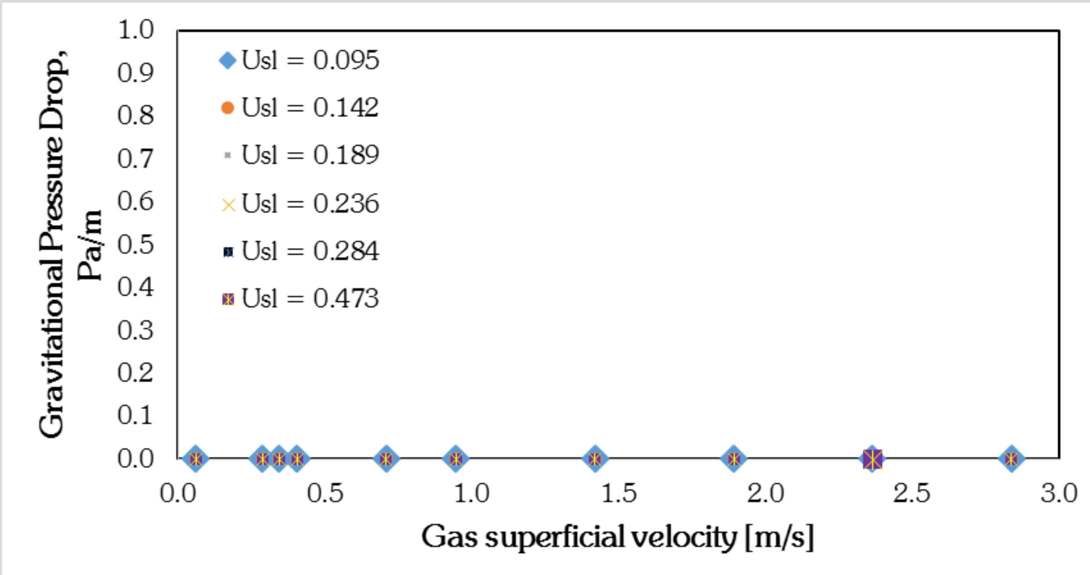

(a)

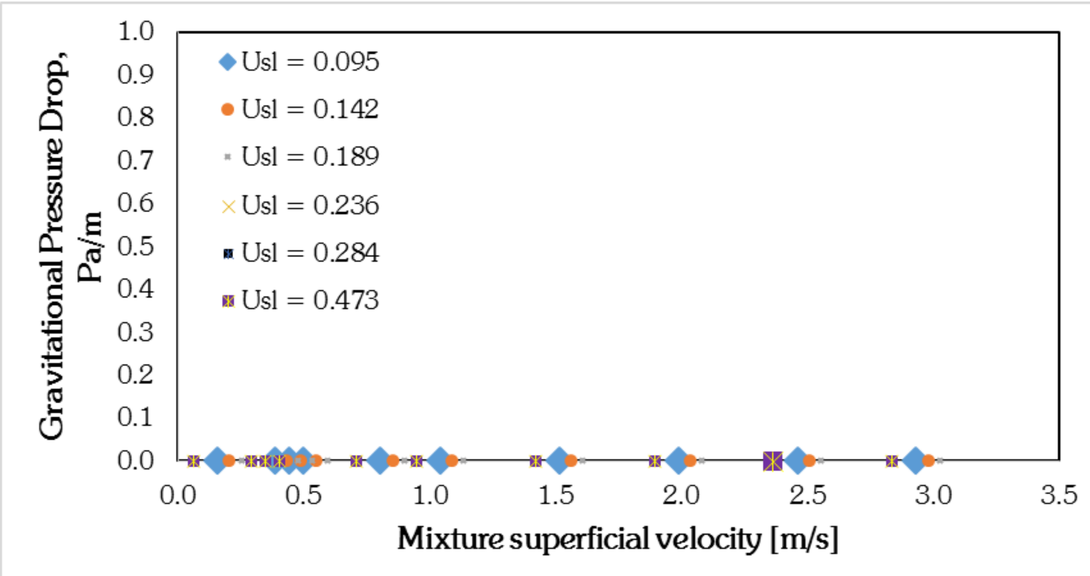

(b)

Figure 4.10: Influence of gas and mixture superficial velocities on the gravitational pressure drop at different liquid superficial velocities

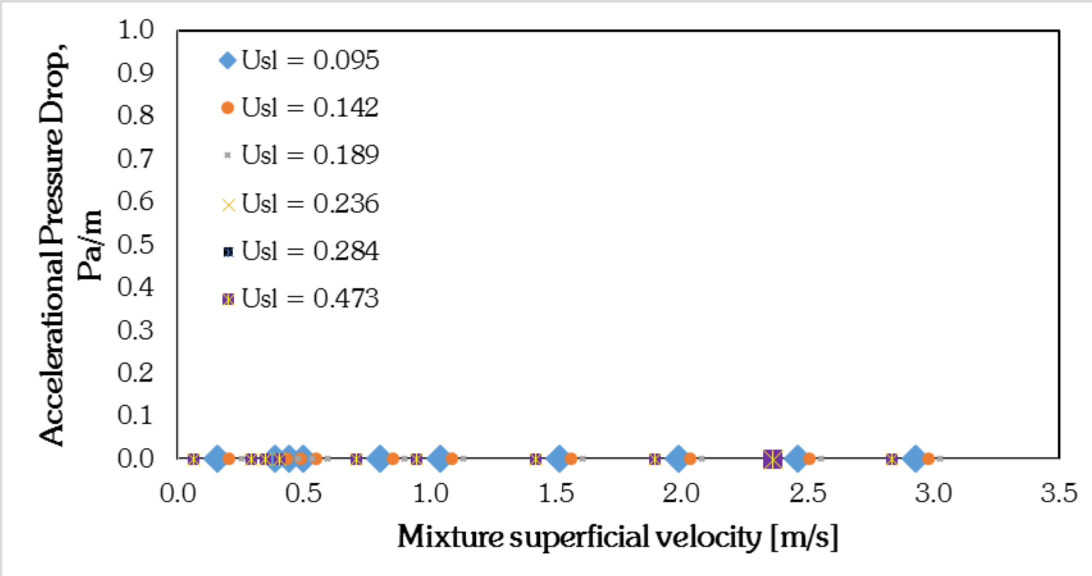

(a)

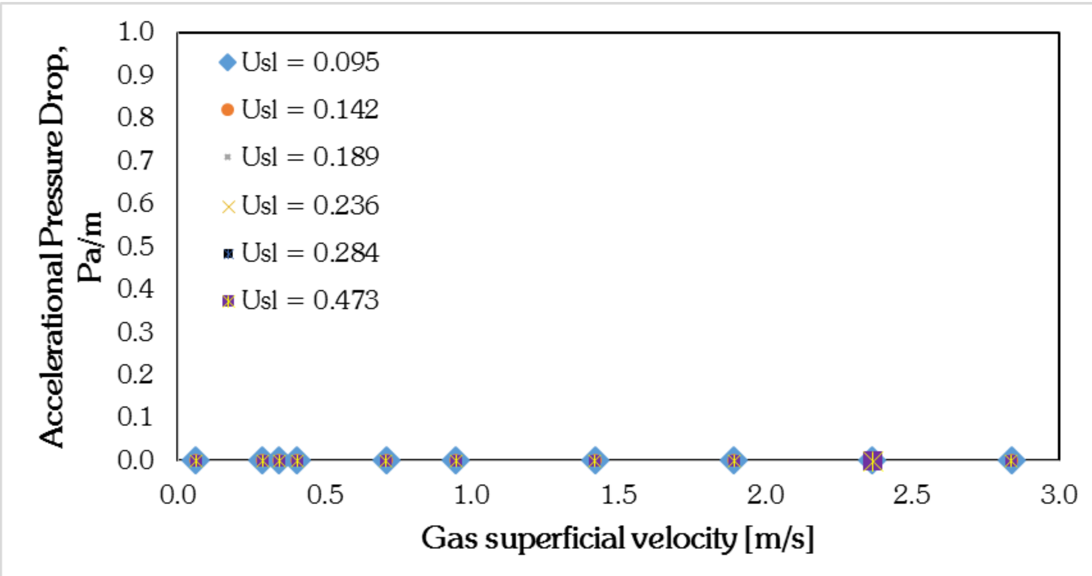

(b)

Figure 4.11: **Influence of gas and mixture superficial velocities on the accelerational pressure drop at different liquid superficial velocities**

It is interesting to note that for a given liquid superficial velocity, the frictional pressure drop increases with increase in both gas and mixture superficial velocities. This increase can be attributed to the fact that flow in horizontal pipe is friction dominated, as there is zero static pressure (gravitational pressure) drop, whilst the accelerational pressure drop is also negligibly very small. This signifies that the lower the mixture density, the higher the frictional pressure drop, hence, the higher the total pressure drop will be. Also, having a closer look at the variation of the frictional pressure drop (the main contributor to the total pressure drop) with liquid superficial velocity, it was obseved that as the liquid superficial velocity increases, the frictional pressure drop also increases. This can be attributed to the increase in shear stress between the liquid and the walls of the tube and comparatively larger bubbles are observed to form due to coalescence, which causes a decrease in the liquid velocity due to higher level of liquid holdup, hence increasing the frictional pressure drop. These observations support the phenomena reported by Beggs and Brill (1973) and Dukler and Hubbard (1975).

4.7 Effect of gas superficial velocity on the dominant frequency

In order to determine the frequency of periodic structures the methodology of Power Spectral Density (PSD) was applied. The Power Spectral Density, PSD, is a measure of how the power in a signal changes over frequency and therefore, it describes how the power (or variance) of a time series is distributed with frequency. The results obtained showed that;

At liquid velocity of 0.047 m/s, the frequency increased at lower gas superficial gas velocity and decresed upto a point and remained contant as the gas superficial velocity increased and then decresed with further increase in the gas superficial velocity to a minimum of 0.017 Hz. This same trend could be said of the liquid superficial velocity of 0.095 m/s but in this case to minimum of 0.033 Hz and increased to 0.049 Hz. It can also be observed from figure 4.12b that the frequency assumes a sinusoidal trend with increase in the gas superficial velocity. This behaviour can be linked to the probabilty density function plots as shown in figure 4.7 of the cross-sectionally averaged time series of void fraction and can be concluded that these different trends can be attributed to the change in flow pattern. It can also be observed that an increase in liquid superficial velocity is responsible for an increase in the frequency as it has been reported in the literature for horizontal flow, Manolis et al. (1995). This behaviour is illustrated clearly in Figure 4.12 a&b.

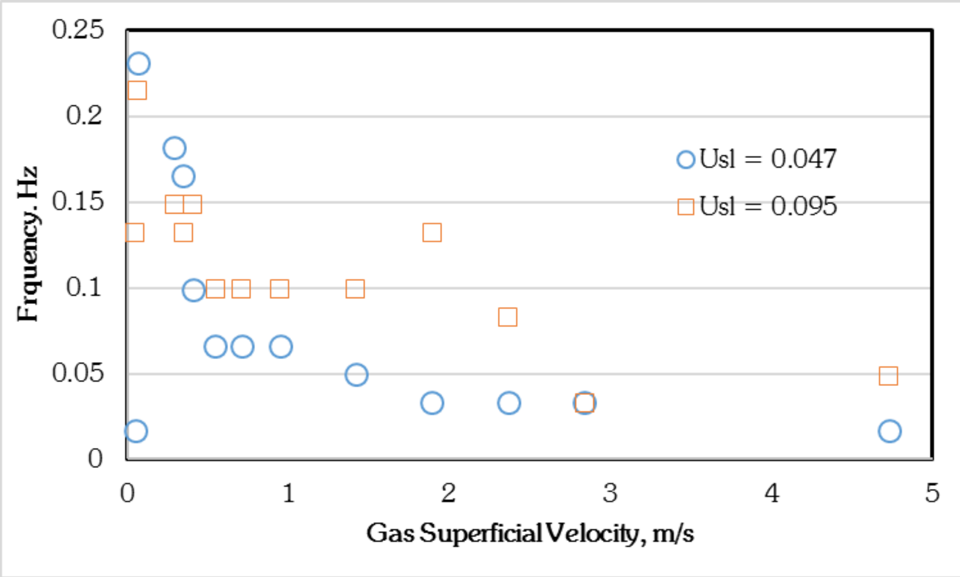

Figure 4.12a: Effect of U_{SG} on frequency

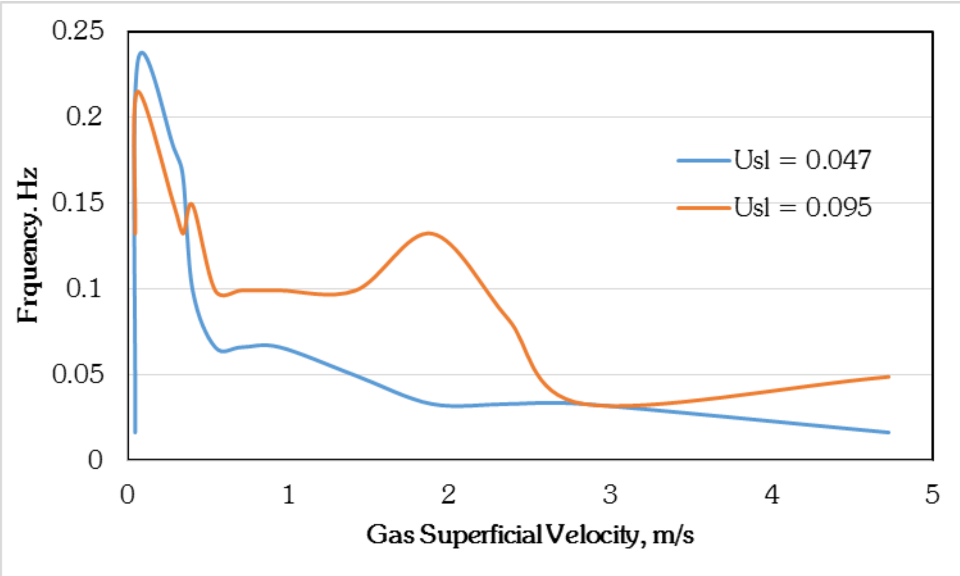

Figure 4.12b: Effect of U_{SG} on frequency

±

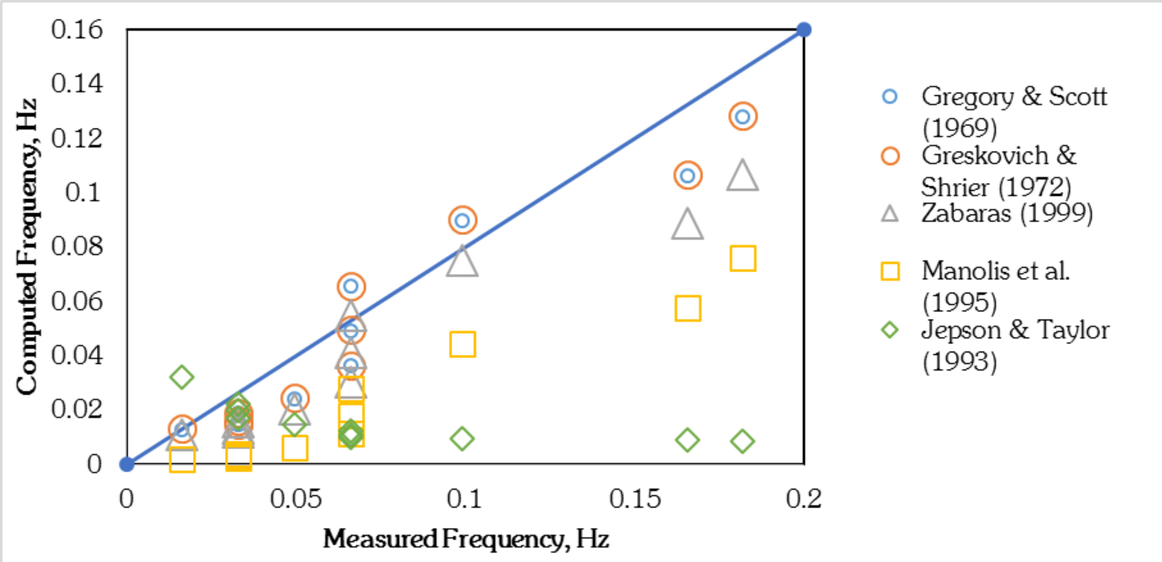

Figure 4.13: Comparison of frequency correlations at USL=0.047 m/s.

In order to examine the prediction of the frequency measured in the present study with respect to different physical models and correlations, the following models were examined for the horizontal case. The comparison is shown in Figures 4.13 and 4.14. It can be observed that the Gregory and Scott (1969) and Greskovich and Shrier (1972) models gave identical results and almost assumed the same trend as the experimental as can be observed from Figure 4.14. Here, the frequences decreases with increase in the gas superficial velocity.

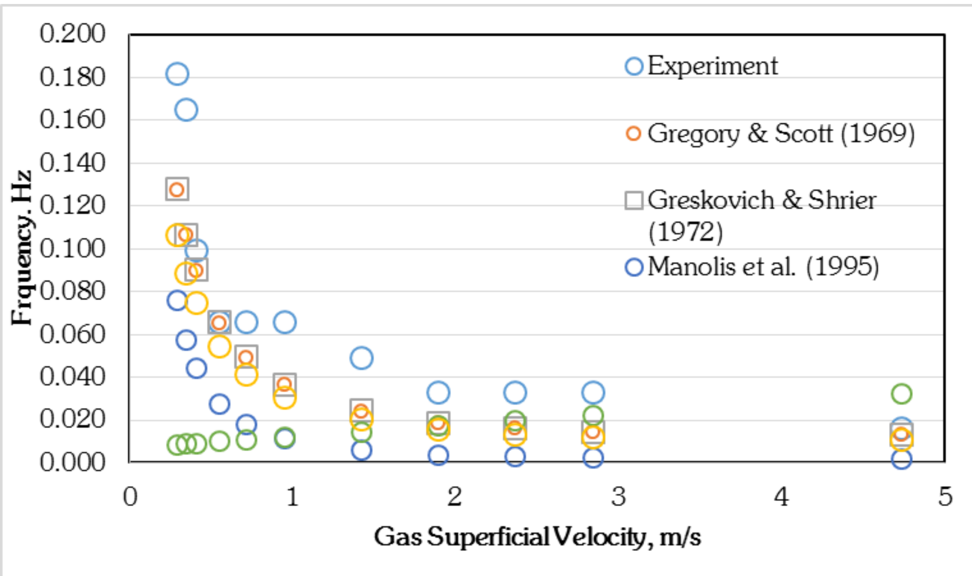

Figure 4.14: Effect of USG on frequency correlation at USL=0.047 m/s.

Table 4.2 Comparison of frequency correlations

Correlation	Mean Error (%)	Standard Deviation
Gregory and Scott (1969)	± 29	76
Greskovich and Shrier (1972)	± 29	76
Zabaras (1999)	± 62	83
Manolis et al. (1995)	± 347	360
Jepson & Taylor (1993)	± 502	529

From Table 4.2, based on the mean error and standard deviation discrimination, Gregory and Scott (1969) and Greskovich and Shrier (1972) is adjudged to be best model to predict the experimental frequency in this present study. However critical observation on the standard deviation shows that none of these correlations work well for the experimental frequencies. The comparison might be subjective since it depends on different factors such as the flow conditions.

For that reason, using these frequency correlations for further estimate of other parameters such as slug length may deviate the result one or several orders of magnitude.

CHAPTER 5
CONCLUSIONS AND RECOMMENDATIONS

5.1 CONCLUSIONS

The scope of this work was to make detailed analysis of phase distribution in a horizontal pipe. This detailed analysis has been successfully carried out. Data obtained from wire mesh sensor (WMS) were used for the analyses. The operating fluid considered was an air/silicone oil mixture within a 6 m horizontal pipe with internal diameter of 0.067 m. The gas superficial velocities considered spans from 0.047 to 4.727 m/s, whilst liquid superficial velocities ranged from 0.047 to 0.4727 m/s. The wire mesh sensor (WMS) data obtained consist of the average cross-sectional and time average radial void fraction sensor with an acquisition frequency of 1000 Hz over an interval of 60 s. An analysis of the results shows that:

(1) The major flow patterns observed in this study were found to be in slug and smooth stratified flow regime with the slug flow been the dominant one and which is also consistent with those reported in the literature.

(2) At constant liquid superficial velocity, the void fraction increases with an increase in the gas superficial velocity. However, the average void fraction increases with a decrease in liquid superficial velocity. This observed trend in the horizontal void fraction is consistent with the observations made by (Abdulkadir et al., 2014) and (Abdulkadir et al., 2010) which were all in the vertical orientation.

(3) The performance of the void fraction correlations and their accuracies were judged in terms of percentage error and RMS error. Based on these results and the outcome of the performance analysis of the correlations, Nicklin et al. (1962), Hassan (1995) and Kokal and Stanislav (1989) are judged as the best performing correlations based on both RMS error and percentage error while Greskovich and Cooper (1975)

correlation is judged to have the least accuracy and performance based on both RMS and percentage error.

(4) The radial void fraction increases with gas superficial velocity and that the shape of the profile is dependent on gas superficial velocity. The profiles for plug flow did not follow a similar trend as the slug and stratified wavy flow.

(5) For a given liquid superficial velocity, the frictional pressure drop increases with increase in both gas and mixture superficial velocities. This increase can be attributed to the fact that flow in horizontal pipe is friction dominated, as there is zero static pressure (gravitational pressure) drop, whilst the accelerational pressure drop is also negligibly very small.

(6) Another finding made was that, even though Wu et al. (2001)'s model was proposed for vertical orientation with air and water used as the operating fluid, it could as well replicate the observed radial void fraction in the horizontal orientation even with air and silicone oil used as the operating fluid at both low and high gas superficial velocities.

(7) The experimental frequency was seen to increase with liquid superficial velocity but followed a sinusoidal trend with increase in gas superficial velocity. It was also concluded that none of the correlations could best predict the experimental data based on their mean square error and standard deviation even though Gregory and Scott (1969) and Greskovich and Shrier (1972) correlations were better relative to the others.

5.2 RECOMMENDATIONS

Although an extensive studies have been performed on phase distributions of gas-liquid flow experienced in a horizontal pipe, there are still some issues that need further investigation:

(1) Since Wire Mesh Sensor (WMS) data was used for this present study, future works should consider the use of Electrical Capacitance Tomography (ECT).

(2) Larger pipe diameter should be tested in order to better characterise the effect of pipe diameter on the two-phase mixture parameters such as flow pattern and void fraction.

(3) Experiments on pressure drop should be carried out for lower and higher flow rates both of gas and liquid. Such experimental pressure drop data should be used for the pressure drop analysis.

NOMENCLATURE

D	Diameter of pipe
g	Acceleration of gravity
U_{SG}	Superficial gas velocity
U_{SL}	Superficial liquid velocity
J_L	Superficial liquid velocity
J_G	Superficial gas velocity
$\dot{m}_L$	mass velocity of liquid phase
$\dot{m}$	mass velocity
Fr_G	Gas Froude number
T	Temperature
Re_k	Reynold number
A_G	Area of vapour phase
A_L	Area of Liquid phase
A	Cross sectional area
R_L	Liquid hold up
m_G	mass of vapour phase
m_M	mass of mixture
S	Slip ratio
U_G	Velocity of gas
U_L	Velocity of liquid
α_H	No slip (homogeneous) void fraction
ρ	Density
Fr	Froude number
U_{GM}	Drift velocity
U_M	Mixture velocity
C_o	Distribution parameter

x	quality, mass of vapor/total mass
V_g	Velocity of gas
G	Mass flux
n	steepness of the holdup profile
c	value of gas holdup near the wall
Re_G	Reynolds number, gas
N	Number of data set
RMS	Root mean square
R	radial time
k	Mean velocity in each phase
L_G	Length of vapour phase
L_L	Length of liquid phase

Greek Symbols

λ	Input liquid content,
ψ	Dimensionless liquid phase parameter, Dimensionless
σ	Surface tension
α	Void fraction, average
θ	Pipe inclination angle
ρ_L	Density of liquid
ρ_G	Density of gas
μ_L	Viscosity of Liquid
μ_G	Viscosity of gas
ρ_{air}	Density of air
ρ_{water}	Density of water
σ_{water}	Surface tension of water
μ_{water}	Viscosity of water
ε_{vol}	volumetric void fraction

$\bar{\varepsilon}_G$	cross-sectional mean gas holdup
$\bar{\varepsilon}$	radial chordal average gas holdup
$\alpha_{predicted}$	Predicted void fraction
$\alpha_{measured}$	Measured void fraction
ε	Void fraction
$\varepsilon_{chordal}$	chordal void fraction

Subscripts

acc	Accelerational
fric	Frictional
grav	Gravitational
d	Drift
eff	Effective
G	Gas
L	Liquid
H	Horizontal
vol	Volumetric
SG	Gas Superficial
SL	Liquid Superficial

REFERENCES

Abdulkadir, M. Hernandez-Perez, V., S. Sharaf, I.S. Lowndes, B.J. Azzopardi, Experimental investigation of phase distributions of two-phase air–silicone oil flow in a vertical pipe, World Acad. Sci. Eng. Technol. (WASET) 61 (2010) 52– 59.

Abdulkadir, M., Hernandez-Perez, V., Detailed analysis of phase distributions in a vertical riser using wire mesh sensor (WMS),

Anglart, H. and Podowski, M. Z., "Fluid Mechanics of Taylor Bubbles and Slug Flows in Vertical Channels," Nuclear Science and Engineering, 140, 165-171 (2002).

Armand, A.A. (1946), "The resistance during the movement of a two-phase system in horizontal pipes," Izv Vse Tepl Inst, Vol. 1,pp. 16-23.

Azzopardi, B.J., Hernandez-Perez, V., Kaji, R., M.J. da Silva, M. Beyer, U. Hampel, Wire mesh sensor studies in a vertical pipe, in: HEAT 2008, Fifth International Conference on Multiphase Systems, Bialystok, Poland, 2008.

Baker, O. (1954), Design of pipelines for the simultaneous flow of oil and Gas, Oil and Gas Journal, Vol.26, pp.185-195.

Bankoff, S.G. (1960), A variable density single fluid model for two phase flow with particular reference to steam water flow, Transactions the ASME, Journal of Heat Transfer, Vol.82, pp.265-272.

Beggs, H.D., An Experimental Study of Two Phase Flow in Inclined Pipes. PhD Thesis, University of Tulsa, Tulsa, 1972.

Bhagwat, S.M., Ghajar, A.J., Similarities and differences in the flow patterns and void fraction in vertical upward and downward two phase flow, Exp. Therm. Fluid Sci. 39 (2012) 213–227.

Brill, J. P., “Multiphase flow in wells,” SPE 16242, Journal of Petroleum Technology, Jan., 15-21 (1987).
Brown, K. E., The Technology of Artificial Lift Methods, PennWell Publishing Co., Tulsa, OK. 1, (1977).

Clark, N.N., Flemmer, R.L., Predicting the holdup in two-phase bubble upflow and downflow using the Zuber and Findlay Drift Flux model, AIChE 31 (3) (1985) 500-503.

Clarke, A., Issa, R. I., “Numerical Model of Slug Flow in Vertical Tubes,” Computers & Fluids, 26 (4), 395-415 (1997).

Costigan, G., Whalley, P.B., Slug flow regime identification from dynamic void fraction measurements in vertical air–water flows, Int. J. Multiphase Flow 23 (1997) 263–282.

Fernandes, R. C. et al., “Hydrodynamic Model for Gas-Liquid Slug Flow in Vertical Tubes," AIChE Journal, 29 (6), 981-989 (1983).

Golan, L., An Air–Water Study of Vertical Upward and Downward Two Phase Flow. PhD Thesis, Leigh University, 1968.

Gomez, L. E. et al., “A Unified Mechanistic Model for Steady-State Two-Phase Flow in Wellbores and Pipelines,” SPE Annual Technological Conference Exhibition, Houston, Texas, USA, SPE 56520, (1999).

Greskovich, E.J., Cooper, W.T., Correlation and prediction of gas–liquid holdups in inclined upflows, AIChE J. 21 (1975) 1189–1192.

Hasan, A.R., Void fraction in bubbly and slug flow in downward vertical and inclined systems, Soc. Petrol. Eng. Prod. Facil. 10 (3) (1995) 172–176.

Isbin, H.S. and Biddle, D. (1979), Void fraction relationships for upward flow of saturated, steam-water mixtures, International Journal of Multiphase Flow, Vol.5, pp.293-299.

Johnson, I.D., Method and apparatus for measuring water in crude oil, us patent. (4644263), 1987.

Kawaji, M. et al., “Investigation of Flow Structures in Vertical Slug Flow,” Nuclear Engineering and Design,” 175, 37-48 (1997).

Kokal, S.L. and Stanislav, J.F. (1989), an experimental study of two phase flow in slightly inclined pipes-II. Liquid holdup and pressure drop, Chemical Engineering Science, Vol.44, No.3, pp.681-693.

Kokal, S.L., Stainslav, J.F., An experimental study of two phase flow in slightly inclined pipes II: liquid holdup and pressure drop, Chem. Eng. Sci. 44 (1989) 681–693.

Manera, A., Ozar, B., Paranjape, S., Ishii, M., Prasser, H.-M., Comparison between wire-mesh-sensors and conducting needle-probes for measurements of two phase flow parameters, Nucl. Eng. Des. 239 (2008) 1718–1724.

Morooka, S., Ishizuka, T., Iizuka, M., Yoshimura, K., Experimental study on void fraction in a simulated BWR fuel assembly (evaluation of cross-sectional averaged void fraction), Nucl. Eng. Des. 114 (1989) 91–98.

Mukherjee, H., An Experimental Study of Inclined Two Phase Flow. PhD Thesis, The University of Tulsa, Tulsa, 1979.

Nguyen, V.T., Two Phase Gas–Liquid Cocurrent Flow: An Investigation of Hold Up, Pressure Drop and Flow Pattern in a pipe at Various Inclinations. PhD Thesis, The University of Auckland, 1975.

Nicklin, D.J., Wilkes, J.O. and Davidson, J.F. (1962), Two-phase flow in vertical tubes, Transactions of the Institution of Chemical Engineers, Vol.40, pp.61- 68.

Ohnuki, A., Akimoto, H., An experimental study on developing air–water two phase flow along a large vertical pipe: effect of air injection method, Int. J. Multiphase Flow 22 (6) (1996) 143–1154.

Ohnuki, A., Akimoto, H., Experimental study on transition of flow pattern and phase distribution in upward air–water two-phase flow along a large vertical pipe, Int. J. Multiphase Flow 26 (3) (2000) 367–386.

Orell, A., and Rembrand, R., “A Model for Gas-Liquid Slug Flow in a Vertical Tube,” Ind. Eng. Chem. Fundam., 25, 196-206 (1986).

Oshinowo, T., Charles, M.E., Vertical two-phase flow – Part 1: Flow pattern correlations, Can. J. Chem. Eng. 52 (1974) 25–35.

Prasser, H.-M., Böttger, A. and Zschau, J. A new electrode-mesh tomograph for gas liquid flows. Flow Measurement and Instrumentation, 9:111–119, 1998.

Prasser, H.-M., Krepper, E., Lucas, D., Evolution of the two-phase flow in a vertical tube-decomposition of gas fraction profiles according to bubble size classes using wire mesh sensors, Int. J. Therm. Sci. 41 (2002) 17–28.

Prasser, H.-M., Misawa, M. and Tiseanu, I., Comparison between wire-mesh sensor and ultra-fast x-ray tomograph for an air-water flow in a vertical pipe. Flow Measurement and Instrumentation, 16, 2005.

Shoham, O., Mechanistic Modelling of Gas–Liquid Two-phase Flow in Pipes, University of Tulsa, Society of Petroleum Engineers, USA, 2006.

Sylvester, N. D., "A Mechanistic Model for Two-Phase Vertical Slug Flow in Pipes," Transaction of ASME, 109, 206-213 (1987).

Szalinski, L., Abdulkareem, L.A., M.J. da Silva, S. Thiele, M. Beyer, D. Lucas, V. Hernandez-Perez, U. Hampel, B.J. Azzopardi, Comparative study of gas–oil and gas-water two-phase flow in a vertical pipe, Chem. Eng. Sci. 65 (2010) 3836–3848.

Taylor, G. The dispersion of matter in turbulent flow through a pipe. Proceedings of the Royal Society of London, 223:446–468, 1954.

Taitel, Y., "Advances in Two Phase Flow Mechanistic Modeling," SPE 27959, University of Tulsa Centennial Petroleum Engineering Symposium, Tulsa, Oklahoma, August (1995).

Taitel, Y., and Barnea, D., "Two-Phase Slug Flow," Advances in Heat Transfer, 20, 83-132 (1990).

Taitel, Y., and Barnea, D., "Two-Phase Slug Flow," Advances in Heat Transfer, 20, 83-132 (1990).

Vijayan, P.K., Patil, A.P., Pilkhawal, D.S., Saha, D., Venkat Raj, V. (2000), An assessment of pressure drop and void fraction correlations with data from two phase natural circulation loops, Heat and Mass Transfer, Vol. 36, pp.541-548.

Wallis, G. B., One-dimensional Two-phase Flow. McGraw-Hill, New York, (1969).

Worner, M., “Computation Modeling of Multiphase Flows,” International Summer School on Computational Modeling of Combustion & Multiphase Flows in Energy Systems,” Romania, July (2003).

Zuber, N., J.A. Findlay, Average volumetric concentration in two-phase flow systems, J. Heat Transfer 87 (1965) 453–468.

APPENDIX

Table A1: Processed Data for Comparison of Experimental Frequency with Empirical correlations

RUN	Usl (m/s)	Usg (m/s)	Um (m/s)	Experimental Frequency	Gregory and Scott (1969)	Greskovich and Shrier (1972)	Zabaras (1999)	Nydal (1991)	Fr	Manolis et al. (1995)	Jepson & Taylor (1993)
1	0.047	0.047	0.094	0.017	0.584	0.586	0.488	0.320	19.025	0.743	0.008
2	0.047	0.061	0.108	0.232	0.495	0.497	0.413	0.320	16.560	0.579	0.008
3	0.047	0.288	0.335	0.182	0.128	0.128	0.107	0.320	5.360	0.076	0.009
4	0.047	0.344	0.391	0.166	0.107	0.107	0.089	0.320	4.600	0.058	0.009
5	0.047	0.404	0.451	0.099	0.090	0.090	0.075	0.320	3.996	0.045	0.009
6	0.047	0.544	0.591	0.066	0.066	0.066	0.055	0.320	3.067	0.028	0.010
7	0.047	0.709	0.756	0.066	0.050	0.050	0.041	0.320	2.419	0.018	0.011
8	0.047	0.945	0.992	0.066	0.037	0.037	0.031	0.320	1.873	0.011	0.012
9	0.047	1.418	1.465	0.050	0.024	0.025	0.020	0.320	1.325	0.006	0.015
10	0.047	1.891	1.938	0.033	0.019	0.019	0.016	0.320	1.061	0.004	0.017
11	0.047	2.363	2.41	0.033	0.016	0.016	0.014	0.320	0.914	0.003	0.020
12	0.047	2.836	2.883	0.033	0.015	0.015	0.012	0.320	0.826	0.003	0.022
13	0.047	4.727	4.774	0.017	0.013	0.013	0.011	0.320	0.716	0.002	0.032
14	0.095	0.047	0.142	0.132	0.829	0.832	0.693	0.341	25.467	1.256	0.016
15	0.095	0.061	0.156	0.215	0.741	0.744	0.619	0.341	23.186	1.061	0.016
16	0.095	0.288	0.383	0.149	0.254	0.255	0.212	0.341	9.490	0.212	0.018
17	0.095	0.344	0.439	0.132	0.216	0.217	0.181	0.341	8.295	0.167	0.019
18	0.095	0.404	0.499	0.149	0.186	0.187	0.156	0.341	7.313	0.133	0.020
19	0.095	0.544	0.639	0.099	0.140	0.140	0.117	0.341	5.747	0.086	0.021
20	0.095	0.709	0.804	0.099	0.107	0.108	0.090	0.341	4.611	0.058	0.023
21	0.095	0.945	1.04	0.099	0.081	0.081	0.068	0.341	3.625	0.038	0.025
22	0.095	1.418	1.513	0.099	0.055	0.055	0.046	0.341	2.607	0.021	0.030
23	0.095	1.891	1.986	0.132	0.043	0.044	0.036	0.341	2.107	0.014	0.036
24	0.095	2.363	2.458	0.083	0.037	0.037	0.031	0.341	1.825	0.011	0.041

Table A2: Processed Data for Pressure Drop Computations with Beggs and Brill Approach

RUN	Usl[m/s]	Usg[m/s]	Um[m/s]	ε	H_L	pm	Um	Rem	Constant	Fm	$(dP/dz)_G$	$(dP/dz)_F$	$(dP/dz)_{Acc}$	$(dP/dz)_T$
15	0.095	0.061	0.156	0.377	5.000	4495.100	0.026	1794.713	3.349	0.089	0.000	13.571	0.000	13.571
16	0.095	0.288	0.383	0.496	0.504	454.405	0.003	4390.206	4.086	0.060	0.000	5.555	0.000	5.555
17	0.095	0.344	0.439	0.530	0.470	423.492	0.002	5030.629	4.199	0.057	0.000	6.443	0.000	6.443
18	0.095	0.404	0.499	0.568	0.432	389.266	0.002	5716.002	4.304	0.054	0.000	7.282	0.000	7.282
20	0.095	0.709	0.804	0.658	0.342	308.573	0.002	9198.385	4.697	0.045	0.000	12.585	0.000	12.585
21	0.095	0.945	1.040	0.694	0.306	276.250	0.002	11890.126	4.908	0.042	0.000	17.260	0.000	17.260
22	0.095	1.418	1.513	0.781	0.219	198.057	0.001	17252.580	5.215	0.037	0.000	23.196	0.000	23.196
23	0.095	1.891	1.986	0.792	0.208	188.158	0.001	22635.140	5.439	0.034	0.000	34.907	0.000	34.908
24	0.095	2.363	2.458	0.800	0.200	181.171	0.001	28004.184	5.615	0.032	0.000	48.319	0.000	48.319
25	0.095	2.836	2.931	0.823	0.177	160.181	0.001	33348.982	5.759	0.030	0.000	57.748	0.001	57.749
28	0.142	0.061	0.203	0.170	0.830	747.554	0.004	2330.626	3.564	0.079	0.000	3.374	0.000	3.374
29	0.142	0.288	0.430	0.359	0.641	577.513	0.003	4933.212	4.183	0.057	0.000	8.495	0.000	8.495
30	0.142	0.344	0.486	0.392	0.608	547.764	0.003	5574.711	4.283	0.055	0.000	9.814	0.000	9.814
31	0.142	0.404	0.546	0.446	0.554	498.859	0.003	6260.883	4.379	0.052	0.000	10.793	0.000	10.793
33	0.142	0.709	0.851	0.583	0.417	376.065	0.002	9746.516	4.744	0.044	0.000	16.839	0.000	16.839
34	0.142	0.945	1.087	0.590	0.410	369.723	0.002	12448.383	4.946	0.041	0.000	24.850	0.000	24.850
35	0.142	1.418	1.560	0.706	0.294	265.465	0.002	17830.374	5.243	0.036	0.000	32.711	0.000	32.711
36	0.142	1.891	2.033	0.743	0.257	232.078	0.001	23213.546	5.460	0.034	0.000	44.774	0.000	44.775
37	0.142	2.363	2.505	0.762	0.238	215.018	0.001	28585.099	5.632	0.032	0.000	59.203	0.000	59.204
38	0.142	2.836	2.978	0.758	0.242	218.663	0.001	33987.432	5.774	0.030	0.000	80.941	0.001	80.942
41	0.189	0.061	0.250	0.118	0.882	793.891	0.005	2870.642	3.736	0.072	0.000	4.947	0.000	4.947
42	0.189	0.288	0.477	0.320	0.680	612.484	0.004	5473.420	4.268	0.055	0.000	10.646	0.000	10.646
43	0.189	0.344	0.533	0.355	0.645	580.713	0.003	6114.996	4.360	0.053	0.000	12.080	0.000	12.080
44	0.189	0.404	0.593	0.393	0.607	546.881	0.003	6802.028	4.448	0.051	0.000	13.530	0.000	13.530
46	0.189	0.709	0.898	0.505	0.495	445.760	0.003	10292.677	4.789	0.044	0.000	21.810	0.000	21.810

47	0.189	0.945	1.134	0.565	0.435	391.908	0.002	12990.287	4.981	0.040	0.000	28.265	0.000	28.265
48	0.189	1.418	1.607	0.696	0.304	274.369	0.002	18371.694	5.267	0.036	0.000	35.541	0.000	35.541
49	0.189	1.891	2.080	0.692	0.308	277.716	0.002	23781.085	5.480	0.033	0.000	55.678	0.000	55.679
50	0.189	2.363	2.552	0.701	0.299	269.865	0.002	29171.952	5.648	0.031	0.000	76.663	0.000	76.663
51	0.189	2.836	3.025	0.739	0.261	235.879	0.001	34544.967	5.788	0.030	0.000	89.675	0.001	89.676
54	0.236	0.061	0.297	0.092	0.908	817.311	0.005	3410.550	3.878	0.066	0.000	6.671	0.000	6.671
55	0.236	0.288	0.524	0.279	0.721	649.054	0.004	6013.749	4.346	0.053	0.000	13.132	0.000	13.132
56	0.236	0.344	0.580	0.320	0.680	612.676	0.004	6655.318	4.430	0.051	0.000	14.619	0.000	14.619
57	0.236	0.404	0.640	0.349	0.651	585.982	0.003	7342.793	4.511	0.049	0.000	16.418	0.000	16.418
59	0.236	0.709	0.945	0.479	0.521	469.344	0.003	10833.629	4.832	0.043	0.000	24.987	0.000	24.987
60	0.236	0.945	1.181	0.517	0.483	435.662	0.003	13535.066	5.015	0.040	0.000	33.620	0.000	33.620
61	0.236	1.418	1.654	0.633	0.367	331.355	0.002	18930.795	5.292	0.036	0.000	45.046	0.000	45.046
62	0.236	1.891	2.127	0.687	0.313	282.918	0.002	24321.402	5.499	0.033	0.000	58.915	0.000	58.915
63	0.236	2.363	2.599	0.706	0.294	265.171	0.002	29705.633	5.663	0.031	0.000	77.718	0.000	77.718
64	0.236	2.836	3.072	0.761	0.239	215.840	0.001	35056.396	5.800	0.030	0.000	84.274	0.001	84.275
67	0.284	0.061	0.345	0.057	0.943	848.458	0.005	3962.078	4.002	0.062	0.000	8.776	0.000	8.776
68	0.284	0.288	0.572	0.256	0.744	669.610	0.004	6565.199	4.418	0.051	0.000	15.619	0.000	15.619
69	0.284	0.344	0.628	0.285	0.715	643.979	0.004	7207.157	4.495	0.049	0.000	17.492	0.000	17.492
70	0.284	0.404	0.688	0.340	0.660	594.466	0.003	7893.857	4.570	0.048	0.000	18.748	0.000	18.748
72	0.284	0.709	0.993	0.474	0.526	474.004	0.003	11384.347	4.872	0.042	0.000	27.398	0.000	27.398
73	0.284	0.945	1.229	0.517	0.483	435.467	0.003	14085.152	5.048	0.039	0.000	35.920	0.000	35.920
74	0.284	1.418	1.702	0.625	0.375	338.158	0.002	19482.351	5.316	0.035	0.000	48.245	0.000	48.245
75	0.284	1.891	2.175	0.766	0.234	211.628	0.001	24816.009	5.515	0.033	0.000	45.804	0.000	45.804
76	0.284	2.363	2.647	0.707	0.293	264.361	0.002	30253.614	5.678	0.031	0.000	79.943	0.000	79.944
77	0.284	2.836	3.120	0.764	0.236	213.088	0.001	35600.248	5.812	0.030	0.000	85.446	0.001	85.447
93	0.473	0.061	0.534	0.079	0.921	829.162	0.005	6132.298	4.362	0.053	0.000	17.294	0.000	17.294
94	0.473	0.288	0.761	0.244	0.756	680.906	0.004	8734.869	4.654	0.046	0.000	25.338	0.000	25.338

95	0.473	0.344	0.817	0.262	0.738	664.181	0.004	9377.006	4.712	0.045	0.000	27.783	0.000	27.784
96	0.473	0.404	0.877	0.317	0.683	615.087	0.004	10063.419	4.771	0.044	0.000	28.928	0.000	28.928
98	0.473	0.709	1.182	0.484	0.516	465.145	0.003	13550.154	5.016	0.040	0.000	35.943	0.000	35.943
99	0.473	0.945	1.418	0.535	0.465	419.123	0.002	16248.539	5.166	0.037	0.000	43.946	0.000	43.946
100	0.473	1.418	1.891	0.594	0.406	366.414	0.002	21654.862	5.403	0.034	0.000	62.465	0.000	62.466
101	0.473	1.891	2.364	0.657	0.343	309.354	0.002	27046.404	5.586	0.032	0.000	77.102	0.000	77.102
102	0.473	2.363	2.836	0.716	0.284	256.662	0.002	32407.021	5.735	0.030	0.000	87.344	0.001	87.345
103	0.473	2.836	3.309	0.745	0.255	230.677	0.001	37781.573	5.861	0.029	0.000	102.315	0.001	102.316

Fluid Properties

Mixture Friction Factor (fm)		
Density of liquid (ρL)	900	Kg/m3
Density Gas (ρG)	1.225	Kg/m3
Viscosity of liquid (μL)	0.00525	Kg/ms
Viscosity of gas (μG)	1.789E-05	Kg/ms
Pipe diameter (mm)	0.067	m
Length of pipe (m) = dz	6	m
g	9.81	m/s2
gc	32.174	lb/ft2
Pipe Roughness (ε)	0.0000025	μm
Mixture density		Kg/m3
Mixture Reynold's number		
μm		m/s

Table A3: Void Fraction Empirical Correlations Comparison with Experimental Data

Usl (m/s)	Usg (m/s)	Um (m/s)	ε	Hughmark (1962)	Nicklin et al.(1962)	Ahmad (1964)	Zuber-Findlay (1965)	Bankoff (1960)	Kokal& stanislav (1989)	Hassan (1995)	Greskovich & Cooper (1975)	Cai et al. (1997)	Clark & Flemmer (1987)
0.095	0.061	0.156	0.377	0.322	0.128	0.152	0.347	0.278	0.129	0.133	0.392	0.331	0.166
0.095	0.288	0.383	0.496	0.617	0.384	0.458	0.666	0.535	0.387	0.403	0.753	0.635	0.455
0.095	0.344	0.439	0.530	0.643	0.421	0.502	0.694	0.557	0.424	0.443	0.784	0.662	0.492
0.095	0.404	0.499	0.568	0.665	0.455	0.542	0.717	0.575	0.457	0.479	0.810	0.684	0.525
0.095	0.709	0.804	0.658	0.724	0.565	0.675	0.781	0.626	0.567	0.598	0.882	0.745	0.630
0.095	0.945	1.040	0.694	0.745	0.615	0.735	0.804	0.645	0.616	0.652	0.909	0.767	0.674
0.095	1.418	1.513	0.781	0.769	0.674	0.806	0.830	0.666	0.675	0.716	0.937	0.791	0.725
0.095	1.891	1.986	0.792	0.781	0.708	0.847	0.843	0.676	0.709	0.753	0.952	0.804	0.754
0.095	2.363	2.458	0.800	0.788	0.730	0.874	0.851	0.683	0.730	0.778	0.962	0.811	0.772
0.095	2.836	2.931	0.823	0.794	0.745	0.893	0.856	0.687	0.746	0.795	0.968	0.817	0.785
0.142	0.061	0.203	0.170	0.247	0.114	0.107	0.266	0.214	0.115	0.119	0.301	0.254	0.144
0.142	0.288	0.430	0.359	0.549	0.357	0.361	0.593	0.476	0.359	0.375	0.670	0.565	0.418
0.142	0.344	0.486	0.392	0.581	0.394	0.403	0.627	0.503	0.396	0.414	0.708	0.598	0.456
0.142	0.404	0.546	0.446	0.607	0.428	0.442	0.655	0.526	0.429	0.450	0.740	0.625	0.490
0.142	0.709	0.851	0.583	0.683	0.541	0.582	0.737	0.592	0.543	0.572	0.833	0.703	0.600
0.142	0.945	1.087	0.590	0.713	0.593	0.650	0.769	0.617	0.594	0.629	0.870	0.734	0.648
0.142	1.418	1.560	0.706	0.745	0.656	0.736	0.805	0.645	0.657	0.698	0.909	0.767	0.705
0.142	1.891	2.033	0.743	0.763	0.693	0.788	0.823	0.660	0.694	0.738	0.930	0.785	0.737
0.142	2.363	2.505	0.762	0.774	0.717	0.823	0.835	0.670	0.718	0.764	0.943	0.796	0.758
0.142	2.836	2.978	0.758	0.781	0.734	0.848	0.843	0.676	0.735	0.783	0.952	0.804	0.773
0.189	0.061	0.250	0.118	0.200	0.103	0.083	0.216	0.173	0.104	0.108	0.244	0.206	0.127
0.189	0.288	0.477	0.320	0.495	0.334	0.298	0.534	0.429	0.336	0.351	0.604	0.509	0.387
0.189	0.344	0.533	0.355	0.529	0.370	0.337	0.571	0.458	0.372	0.390	0.645	0.545	0.425

0.189	0.404	0.593	0.393	0.559	0.403	0.374	0.603	0.484	0.405	0.425	0.681	0.575	0.459
0.189	0.709	0.898	0.505	0.647	0.518	0.512	0.699	0.561	0.520	0.549	0.789	0.666	0.573
0.189	0.945	1.134	0.565	0.683	0.572	0.583	0.737	0.592	0.574	0.607	0.833	0.703	0.625
0.189	1.418	1.607	0.696	0.724	0.639	0.677	0.781	0.626	0.640	0.680	0.882	0.745	0.686
0.189	1.891	2.080	0.692	0.745	0.679	0.736	0.805	0.645	0.680	0.723	0.909	0.767	0.722
0.189	2.363	2.552	0.701	0.759	0.705	0.777	0.819	0.657	0.706	0.752	0.926	0.781	0.745
0.189	2.836	3.025	0.739	0.769	0.723	0.807	0.830	0.666	0.724	0.772	0.937	0.791	0.761
0.236	0.061	0.297	0.092	0.168	0.094	0.067	0.182	0.146	0.095	0.099	0.205	0.173	0.114
0.236	0.288	0.524	0.279	0.450	0.313	0.254	0.486	0.390	0.315	0.330	0.549	0.464	0.360
0.236	0.344	0.580	0.320	0.486	0.349	0.290	0.525	0.421	0.350	0.368	0.593	0.500	0.398
0.236	0.404	0.640	0.349	0.517	0.382	0.324	0.558	0.448	0.383	0.403	0.631	0.532	0.432
0.236	0.709	0.945	0.479	0.615	0.498	0.457	0.664	0.533	0.499	0.527	0.750	0.633	0.549
0.236	0.945	1.181	0.517	0.656	0.553	0.528	0.708	0.568	0.555	0.587	0.800	0.675	0.603
0.236	1.418	1.654	0.633	0.703	0.623	0.627	0.759	0.609	0.624	0.663	0.857	0.723	0.668
0.236	1.891	2.127	0.687	0.729	0.665	0.691	0.787	0.631	0.666	0.709	0.889	0.750	0.707
0.236	2.363	2.599	0.706	0.745	0.693	0.737	0.804	0.645	0.694	0.739	0.909	0.767	0.732
0.236	2.836	3.072	0.761	0.757	0.713	0.771	0.817	0.655	0.714	0.761	0.923	0.779	0.750
0.284	0.061	0.345	0.057	0.145	0.087	0.057	0.157	0.126	0.087	0.091	0.177	0.149	0.104
0.284	0.288	0.572	0.256	0.413	0.295	0.222	0.446	0.358	0.296	0.311	0.504	0.425	0.337
0.284	0.344	0.628	0.285	0.449	0.330	0.254	0.485	0.389	0.331	0.348	0.548	0.463	0.374
0.284	0.404	0.688	0.340	0.482	0.362	0.286	0.520	0.417	0.364	0.383	0.588	0.496	0.408
0.284	0.709	0.993	0.474	0.586	0.479	0.412	0.632	0.507	0.480	0.507	0.714	0.603	0.526
0.284	0.945	1.229	0.517	0.631	0.536	0.483	0.681	0.546	0.537	0.569	0.769	0.649	0.582
0.284	1.418	1.702	0.625	0.683	0.608	0.584	0.737	0.592	0.609	0.647	0.833	0.703	0.651
0.284	1.891	2.175	0.766	0.713	0.652	0.652	0.770	0.617	0.653	0.695	0.870	0.734	0.693
0.284	2.363	2.647	0.707	0.732	0.682	0.700	0.790	0.634	0.683	0.727	0.893	0.753	0.720
0.284	2.836	3.120	0.764	0.745	0.703	0.737	0.805	0.645	0.704	0.750	0.909	0.767	0.739

0.473	0.061	0.534	0.079	0.094	0.066	0.035	0.101	0.081	0.066	0.069	0.114	0.096	0.075
0.473	0.288	0.761	0.244	0.310	0.239	0.147	0.335	0.269	0.240	0.253	0.379	0.319	0.268
0.473	0.344	0.817	0.262	0.345	0.271	0.170	0.373	0.299	0.272	0.287	0.421	0.355	0.301
0.473	0.404	0.877	0.317	0.378	0.301	0.194	0.408	0.327	0.302	0.319	0.461	0.389	0.333
0.473	0.709	1.182	0.484	0.492	0.415	0.297	0.531	0.426	0.416	0.441	0.600	0.506	0.452
0.473	0.945	1.418	0.535	0.547	0.475	0.361	0.590	0.473	0.476	0.504	0.667	0.563	0.512
0.473	1.418	1.891	0.594	0.615	0.554	0.458	0.664	0.533	0.555	0.590	0.750	0.633	0.591
0.473	1.891	2.364	0.657	0.656	0.605	0.530	0.708	0.568	0.606	0.645	0.800	0.675	0.641
0.473	2.363	2.836	0.716	0.683	0.640	0.585	0.737	0.592	0.641	0.683	0.833	0.703	0.674
0.473	2.836	3.309	0.745	0.703	0.666	0.629	0.759	0.609	0.666	0.710	0.857	0.723	0.699

Table A4: Radial Time Average % Void Fraction

Radius (mm)	r/ R	Run 14	Run 15	Run 16	Run 17	Run 18	Run 20	Run 21	Run 22	Run 23	Run 24	Run 25
0.8	0.0	7.2	10.9	59.0	66.3	71.8	81.2	83.0	95.8	97.2	97.8	99.0
2.5	0.1	7.5	11.1	58.5	65.7	71.3	81.1	83.1	95.7	97.2	97.7	99.0
4.2	0.1	9.0	11.9	56.3	63.6	69.3	80.8	83.5	95.5	97.0	97.5	98.7
5.9	0.2	10.6	12.9	54.7	61.7	67.5	80.3	83.5	95.3	96.7	97.1	98.5
7.5	0.2	12.7	14.3	52.8	59.5	65.4	79.6	83.2	94.9	96.1	96.6	98.1
9.2	0.3	19.6	19.8	51.3	58.1	64.1	78.3	82.3	94.6	95.6	95.9	97.7
10.9	0.3	24.8	24.2	50.2	57.0	63.0	77.1	81.5	94.1	95.1	95.3	97.2
12.6	0.4	30.0	29.5	48.5	55.0	61.3	74.8	79.7	92.5	93.7	93.9	95.9
14.2	0.4	33.1	32.7	47.6	53.6	59.8	73.0	78.2	90.7	92.2	92.3	94.3
15.9	0.5	35.4	35.2	47.0	52.5	58.4	71.3	76.5	88.4	90.1	90.3	92.2
17.6	0.5	37.3	37.0	47.3	52.0	57.1	69.4	74.7	85.5	87.1	87.6	89.9
19.3	0.6	38.8	38.4	47.8	51.7	56.2	67.8	73.0	83.0	84.4	85.3	87.9
20.9	0.6	40.2	39.8	48.7	51.8	55.8	65.4	70.6	79.8	81.0	82.2	84.8
22.6	0.7	41.2	40.9	49.3	51.8	55.3	63.9	68.4	77.1	78.1	79.4	82.2
24.3	0.7	42.0	41.8	49.6	51.9	54.9	62.7	66.1	74.1	75.0	76.4	79.5
26.0	0.8	42.7	42.4	49.8	51.9	54.6	61.6	64.5	71.9	72.8	73.9	76.8
27.6	0.8	43.3	43.0	49.8	51.9	54.4	60.8	63.3	70.1	71.0	71.9	74.5
29.3	0.9	43.7	43.5	49.9	51.8	54.1	60.0	62.4	68.6	69.5	70.4	72.6
31.0	0.9	44.0	43.7	49.9	51.7	54.0	59.5	61.7	67.5	68.4	69.1	71.2
32.7	1.0	43.6	43.4	50.1	51.8	54.2	59.5	61.5	67.1	68.1	68.6	70.8

Table A5: Wu et al. (2001)'s published equation compared to the experimental time averaged radial void fraction processed Data

r/ R	ε15	ε16	ε17	ε19	ε21	ε22	ε23	ε24	ε25
0.024	7.293	0.696	0.757	0.872	0.902	1.061	1.095	1.118	1.147
0.076	7.650	0.690	0.752	0.871	0.903	1.060	1.095	1.117	1.146
0.128	9.119	0.667	0.731	0.868	0.908	1.058	1.093	1.114	1.143
0.180	10.811	0.648	0.712	0.863	0.907	1.056	1.089	1.110	1.141
0.229	12.961	0.625	0.689	0.855	0.904	1.051	1.083	1.104	1.137
0.281	19.889	0.611	0.676	0.841	0.894	1.048	1.077	1.096	1.131
0.333	25.230	0.599	0.665	0.828	0.886	1.043	1.071	1.088	1.125
0.385	30.500	0.577	0.646	0.803	0.866	1.025	1.055	1.073	1.109
0.434	33.698	0.563	0.631	0.784	0.849	1.004	1.037	1.054	1.089
0.486	35.979	0.551	0.615	0.766	0.831	0.978	1.013	1.028	1.062
0.538	37.903	0.546	0.602	0.745	0.810	0.944	0.976	0.994	1.031
0.590	39.497	0.542	0.592	0.726	0.791	0.913	0.941	0.960	0.999
0.639	40.881	0.543	0.587	0.699	0.761	0.872	0.894	0.915	0.951
0.691	41.918	0.542	0.581	0.679	0.732	0.832	0.849	0.868	0.902
0.743	42.739	0.540	0.573	0.659	0.697	0.784	0.795	0.810	0.843
0.795	43.377	0.534	0.562	0.634	0.663	0.735	0.740	0.748	0.773
0.844	43.806	0.522	0.546	0.603	0.623	0.679	0.679	0.680	0.697
0.896	43.695	0.496	0.515	0.556	0.567	0.607	0.599	0.594	0.602
0.948	41.983	0.447	0.461	0.485	0.488	0.510	0.497	0.486	0.486
1.000	35.055	0.358	0.367	0.376	0.373	0.380	0.364	0.349	0.344